Article

Cancer Cell

Mitochondrial ClpP-Mediated Proteolysis Induces Selective Cancer Cell Lethality

Highlights

- Activation of the mitochondrial ClpP induces p53-independent cancer cell lethality
- Imipridones are allosteric agonists of ClpP, being tested in human clinical trials
- ClpP activation increases proteolysis of mitochondrial proteins
- ClpP-mediated mitochondrial proteolysis impairs mitochondrial respiratory function

Authors

Jo Ishizawa, Sarah F. Zarabi, R. Eric Davis, ..., Emil F. Pai, Aaron D. Schimmer, Michael Andreeff

Correspondence

aaron.schimmer@uhn.ca (A.D.S.), mandreef@mdanderson.org (M.A.)

In Brief

Ishizawa et al. report that hyperactivating the mitochondrial caseinolytic protease P (ClpP) degrades respiratory chain proteins, disrupts mitochondrial function, and selectively kills cancer cells, regardless of p53 status. They identify imipridones as hyperactivators of ClpP and show their anti-tumor activity.

Ishizawa et al., 2019, Cancer Cell *35*, 721–737
May 13, 2019
https://doi.org/10.1016/j.ccell.2019.03.014

CellPress

Cancer Cell
Article

Mitochondrial ClpP-Mediated Proteolysis Induces Selective Cancer Cell Lethality

Jo Ishizawa,[1,13] Sarah F. Zarabi,[2,3,13] R. Eric Davis,[4] Ondrej Halgas,[2,5] Takenobu Nii,[1] Yulia Jitkova,[2] Ran Zhao,[1] Jonathan St-Germain,[2] Lauren E. Heese,[1] Grace Egan,[2] Vivian R. Ruvolo,[1] Samir H. Barghout,[2,3] Yuki Nishida,[1] Rose Hurren,[2] Wencai Ma,[6] Marcela Gronda,[2] Todd Link,[7] Keith Wong,[2,5] Mark Mabanglo,[5] Kensuke Kojima,[1,8] Gautam Borthakur,[1] Neil MacLean,[2] Man Chun John Ma,[4] Andrew B. Leber,[2] Mark D. Minden,[2,3] Walid Houry,[5,9] Hagop Kantarjian,[10] Martin Stogniew,[11] Brian Raught,[2,3] Emil F. Pai,[2,3,5,12] Aaron D. Schimmer,[2,3,14,*] and Michael Andreeff[1,10,14,15,*]

[1]The University of Texas MD Anderson Cancer Center, Molecular Hematology and Therapy, Department of Leukemia, Houston, TX 77030, USA
[2]Princess Margaret Cancer Centre, University Health Network, Toronto, ON M5G 1L7, Canada
[3]Department of Medical Biophysics, Faculty of Medicine, University of Toronto, Toronto, ON M5G 1L7, Canada
[4]The University of Texas MD Anderson Cancer Center; Department of Lymphoma and Myeloma, Houston, TX 77030, USA
[5]Department of Biochemistry, University of Toronto, Toronto, ON M5S 1A8, Canada
[6]The University of Texas MD Anderson Cancer Center, Bioinformatics and Comp Biology, Houston, TX 77030, USA
[7]The University of Texas MD Anderson Cancer Center, Genomic Medicine, Houston, TX 77030, USA
[8]Saga University, Division of Hematology, Respiratory Medicine and Oncology, Department of Internal Medicine, Saga 849-8501, Japan
[9]Department of Chemistry, University of Toronto, Toronto, ON M5S 3H6, Canada
[10]The University of Texas MD Anderson Cancer Center; Department of Leukemia, Houston, TX 77030, USA
[11]Oncoceutics, Inc., Philadelphia, PA 19104, USA
[12]Department of Molecular Genetics, Faculty of Medicine, University of Toronto, Toronto, ON M5S 1A8, Canada
[13]These authors contributed equally
[14]Senior Author
[15]Lead Contact
*Correspondence: aaron.schimmer@uhn.ca (A.D.S.), mandreef@mdanderson.org (M.A.)
https://doi.org/10.1016/j.ccell.2019.03.014

SUMMARY

The mitochondrial caseinolytic protease P (ClpP) plays a central role in mitochondrial protein quality control by degrading misfolded proteins. Using genetic and chemical approaches, we showed that hyperactivation of the protease selectively kills cancer cells, independently of p53 status, by selective degradation of its respiratory chain protein substrates and disrupts mitochondrial structure and function, while it does not affect non-malignant cells. We identified imipridones as potent activators of ClpP. Through biochemical studies and crystallography, we show that imipridones bind ClpP non-covalently and induce proteolysis by diverse structural changes. Imipridones are presently in clinical trials. Our findings suggest a general concept of inducing cancer cell lethality through activation of mitochondrial proteolysis.

INTRODUCTION

Mitochondria possess their own protein synthesis apparatus, including mitochondrial ribosomes, initiation, and elongation factors. In addition, mitochondria have protein degradation complexes that regulate their protein levels by eliminating excess and/or damaged proteins. At present, at least 15 proteases have been identified in different mitochondrial compartments, including the caseinolytic protease P (ClpP), which is located in the mitochondrial matrix. ClpP is an oligomeric serine protease

Significance

Activation of bacterial ClpP is cytotoxic to Gram-positive cocci, but the effects of mitochondrial ClpP activation on human cancers are not well understood. We demonstrate that hyperactivating ClpP could be a therapeutic strategy for human cancers with increased ClpP, irrespective of p53 mutational status. We also identified imipridones as potent allosteric agonists of human ClpP through extensive biochemical analyses. Through co-crystallography, we defined the precise 3D conformational changes that occur on hyperactivating ClpP with impiridones. We also determined that ClpP activation increases mitochondrial proteolysis and leads to mitochondrial dysfunction. Thus, these data support the clinical development of imipridones, and other ClpP activators, for human cancers with increased ClpP expression.

that is similar to the cytoplasmic/nuclear proteasome (Corydon et al., 1998).

After import into the mitochondria, ClpP is assembled into a double-ringed tetradecameric structure with a hollow chamber containing proteolytic active sites. The tetradecameric structure is capped at each end by an AAA ATPase chaperone, ClpX (de Sagarra et al., 1999). The function of the ClpXP complex in mitochondria is not fully understood, but insights have been gained from its bacterial homolog, which shares structural homology. Bacteria lack a ubiquitin-dependent proteolytic system and instead eliminate intracellular proteins with a family of proteases including the bacterial ClpXP complex. In bacteria, ClpX recognizes and unfolds native substrates and feeds them into the barrel of the ClpP protease for degradation. The bacterial ClpXP complex is responsible for degrading excess proteins including those whose translation stalls on ribosomes.

Recently, we demonstrated that mitochondrial ClpP is overexpressed in 45% of primary acute myeloid leukemia (AML) samples (Cole et al., 2015). ClpP is equally expressed in stem cell and bulk populations, and overexpression occurs across the spectrum of cytogenetic and molecular mutations. ClpP expression is positively correlated with expression of genes related to the mitochondrial unfolded protein response (Cole et al., 2015). Functionally, ClpP maintains the integrity of oxidative phosphorylation as inhibition of the protease results in the accumulation of misfolded or degraded respiratory chain complex subunits and respiratory chain dysfunction in AML cells (Cole et al., 2015). Chemical or genetic inhibition of the protease leads to impaired oxidative phosphorylation and selectively kills AML cells and stem cells over normal hematopoietic cells *in vitro* and *in vivo* (Cole et al., 2015).

In bacteria, naturally occurring antibiotics, acyldepsipeptides (ADEPs), hyperactivate ClpP by binding the protease at its interface with ClpX and opening the pore of the ClpP protease complex (Brotz-Oesterhelt et al., 2005). When activated by ADEPs, ClpP can degrade full-length substrates without its regulatory subunit ClpX. Indeed, these ClpP activators are cytotoxic to a variety of microbial species including dormant bacteria that are responsible for resistant chronic infections (Brotz-Oesterhelt et al., 2005; Conlon et al., 2013). Thus, the activity of ClpP needs to be tightly regulated to maintain cellular homeostasis. Although ClpP activators have been studied in bacteria, the effects of hyperactivating mitochondrial ClpP in malignancies have not been systematically investigated. We therefore investigated the biological and therapeutic effects of mitochondrial ClpP activation in cancers.

RESULTS

Activation of Mitochondrial ClpP Induces Anti-tumor Effects *In Vitro* and *In Vivo*

We tested the anti-cancer effects of ClpP activation by generating a constitutively active ClpP mutant by engineering a point mutation (Y118A) in human ClpP. We selected this site as it is homologous to the Y63A mutation in *S. aureus* ClpP (Figure S1A). The Y63A ClpP mutation in *S. aureus* enlarges the entrance pores of the bacterial enzyme causing activation of the protease (Ni et al., 2016). We purified recombinant Y118A ClpP and found that it had higher enzymatic activity than the wild-type (WT) ClpP in a cell-free enzymatic assay using the fluorogenic protein substrate fluorescein isothiocyanate (FITC)-casein (Leung et al., 2011) (Figure S1B).

To evaluate the effects of this mutation in tumor cells, OCI-AML3 and Z138 cells were transduced with tetracycline-inducible WT or Y118A ClpP, and then treated with tetracycline to induce the expression. Induction of Y118A ClpP, but not WT ClpP, induced apoptosis in a dose-dependent manner (Figure 1A). NSG mice were then injected intravenously with Z138 cells with a tetracycline-inducible Y118A ClpP, and then treated with tetracycline or vehicle. The tetracycline-treated group survived significantly longer than the untreated group (median survival: 48 versus 40 days) (Figure 1B).

As an alternative strategy to test the anti-tumor effects of ClpP activation, we next used acyldepsipeptide 1 (ADEP1). We found that ADEP1 activated the mitochondrial protease and promoted ClpP cleavage of FITC-casein (half maximal effective concentration [EC_{50}] = 21.33 μM; 95% CI: 20.12–22.61) (Figure 1C). We then treated OCI-AML2 cells with ADEP1 and demonstrated that it reduced the growth and viability of these cells with a half maximal inhibitory concentration (IC_{50}) of 50 μM (95% CI: 48.4–51.6) (Figure 1D).

Thus, our data show that activation of mitochondrial ClpP induces lethality in tumor cells *in vitro* and *in vivo*.

The Imipridones ONC201 and ONC212 Potently Activate Mitochondrial ClpP

To find a more potent candidate small-molecule human ClpP activator, we conducted a screen using an in-house library of 747 molecules focused on on-patent and off-patent compounds approved for clinical use or in clinical trials for malignant and non-malignant indications. We screened this library to identify molecules that increased ClpP-mediated cleavage of FITC-casein using a cell-free enzymatic assay (Leung et al., 2011). Under basal conditions, ClpP could not cleave full-length proteins without its chaperone ClpX. However, through this screen, we found that the imipridone ONC201 activated the protease and facilitated ClpP-mediated cleavage of FITC-casein in the absence of ClpX (Figure 2A). ONC201 is a chemical with preclinical efficacy in solid tumors and hematologic malignancies *in vitro* and *in vivo* (Allen et al., 2013, 2016; Ishizawa et al., 2016; Kline et al., 2016; Tu et al., 2017) and it is currently being evaluated in clinical trials in a diverse spectrum of cancers (Arrillaga-Romany et al., 2017; Kline et al., 2016; Stein et al., 2017). ONC212, a more potent derivative of ONC201, is in preclinical evaluation (Lev et al., 2017). Of note, targets that physically bind imipridones and are functionally important for their cytotoxicity have not been identified.

We confirmed that ONC201 activated ClpP without requiring ClpX and induced cleavage of FITC-casein as well as the fluorogenic peptides AC-WLA-AMC, Ac-Phe-hArg-Leu-ACC, and FAPHMALVPC (Clptide), with EC_{50} values of 0.85, 1.67, 0.82, and 3.23 μM, respectively. We also tested the effects of ONC212, ADEP1, and the inactive ONC201 isomer on ClpP activity. ONC212 increased ClpP-mediated cleavage of FITC-casein and AC-WLA-AMC, Ac-Phe-hArg-Leu-ACC, and Clptide, with EC_{50} values of 0.46, 0.18, 0.37, and 3.37 μM, respectively (Figures 2B and S2A). ADEP1 was a less-potent ClpP activator compared with ONC201 and ONC212 (Figure S2A), and the inactive isomer of ONC201 did not increase ClpP-mediated cleavage of its substrates (Figures S2A and S2B). FITC-casein data showed clear positive cooperativity (Gersch et al., 2015) with a Hill coefficient

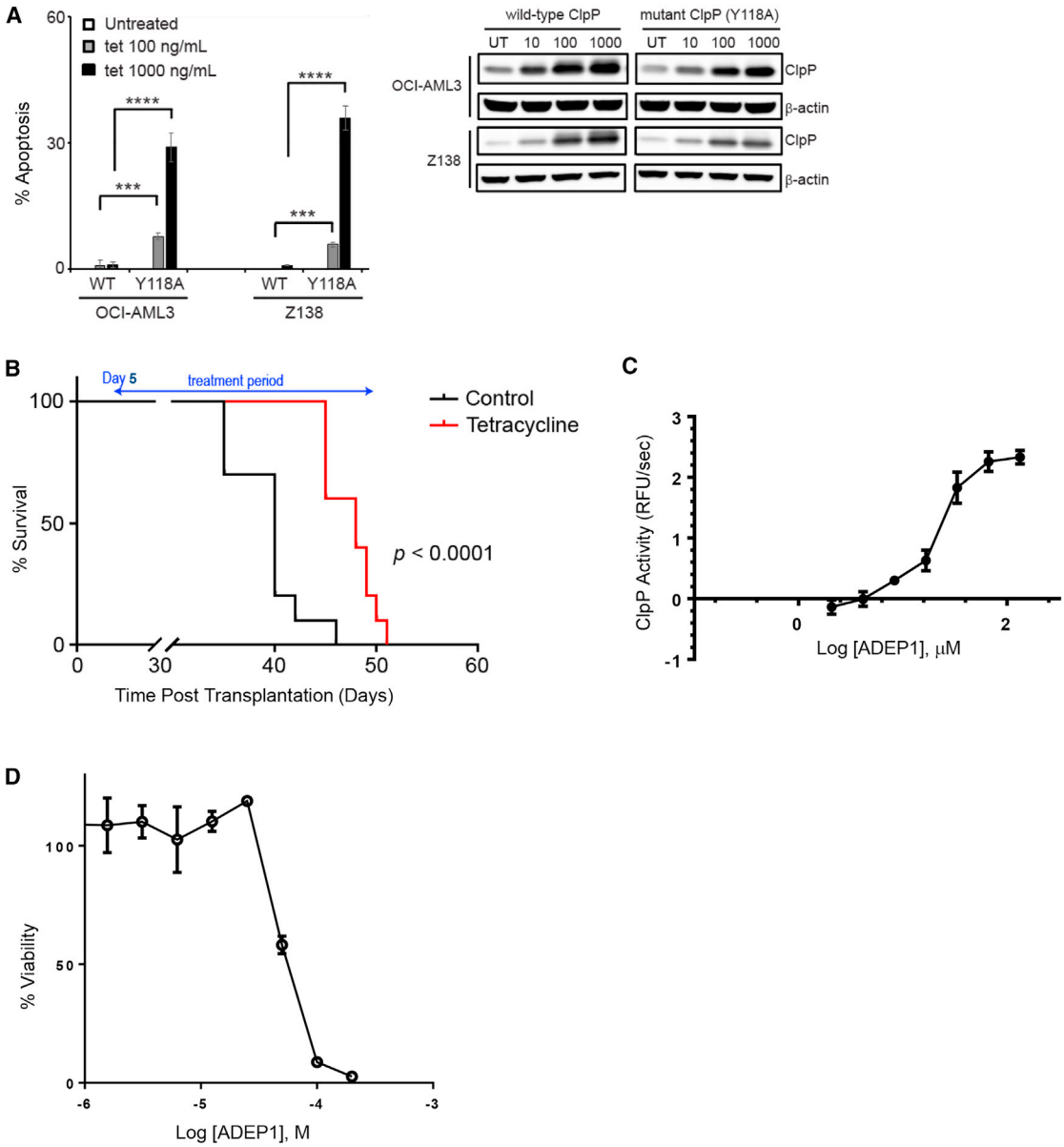

Figure 1. Mitochondrial ClpP Activation Induces Anti-tumor Effects *In Vitro* and *In Vivo*

(A) Quantification for apoptotic (annexin V-positive, left) and immunoblot analysis for the ClpP protein level (right) in OCI-AML3 and Z138 cells with tetracycline-inducible overexpression of WT or Y118A mutant ClpP treated with tetracycline at indicated concentrations for 144 h. The results are expressed as the mean of triplicate samples ±SD (error bars). ***p < 0.001, ****p < 0.0001.

(B) Survivals of xenograft mice using Z138 cells with tetracycline-inducible Y118A mutant ClpP overexpression. The mice (n = 10 each) were treated with or without tetracycline (2 mg/mL in drinking water).

(C) Effects of ADEP1 on degradation of FITC-casein by recombinant WT ClpP. The results are expressed as the mean value of triplicate samples ±SD (error bars).

(D) The viability of OCI-AML2 cells measured by Alamar Blue assay after a 72-h exposure to ADEP1. The results are expressed as the mean value of triplicate samples ±SD (error bars).

See also Figure S1.

of 1.98 ± 0.16 for ONC201 and 4.98 ± 0.47 for ONC212. Notably, the activities of ClpP caused by imipridones were greater than those achieved by the Y118A mutation (Figures S1B and S2A). A non-ClpP substrate, MCA-Pro-Leu-Gly-Pro-D-Lys (DNP)-OH peptide was not cleaved by ClpP treated with imipridones or ADEP1 (Figure S2A). Of note, pre-incubation of ClpP with ONC201 and ONC212 did not increase the activity of ClpP, suggesting a reversible (non-covalent) mode of activation (Figure S2C). As the imipridones were much more potent ClpP activators compared with ADEP1 (Figures 1C and S2D), we focused subsequent studies on these compounds.

To confirm the results of the fluorogenic assays, we tested the effects of ONC201 and ONC212 in a gel-based assay that measures the degradation of α-casein by ClpP (Figure 2D). The

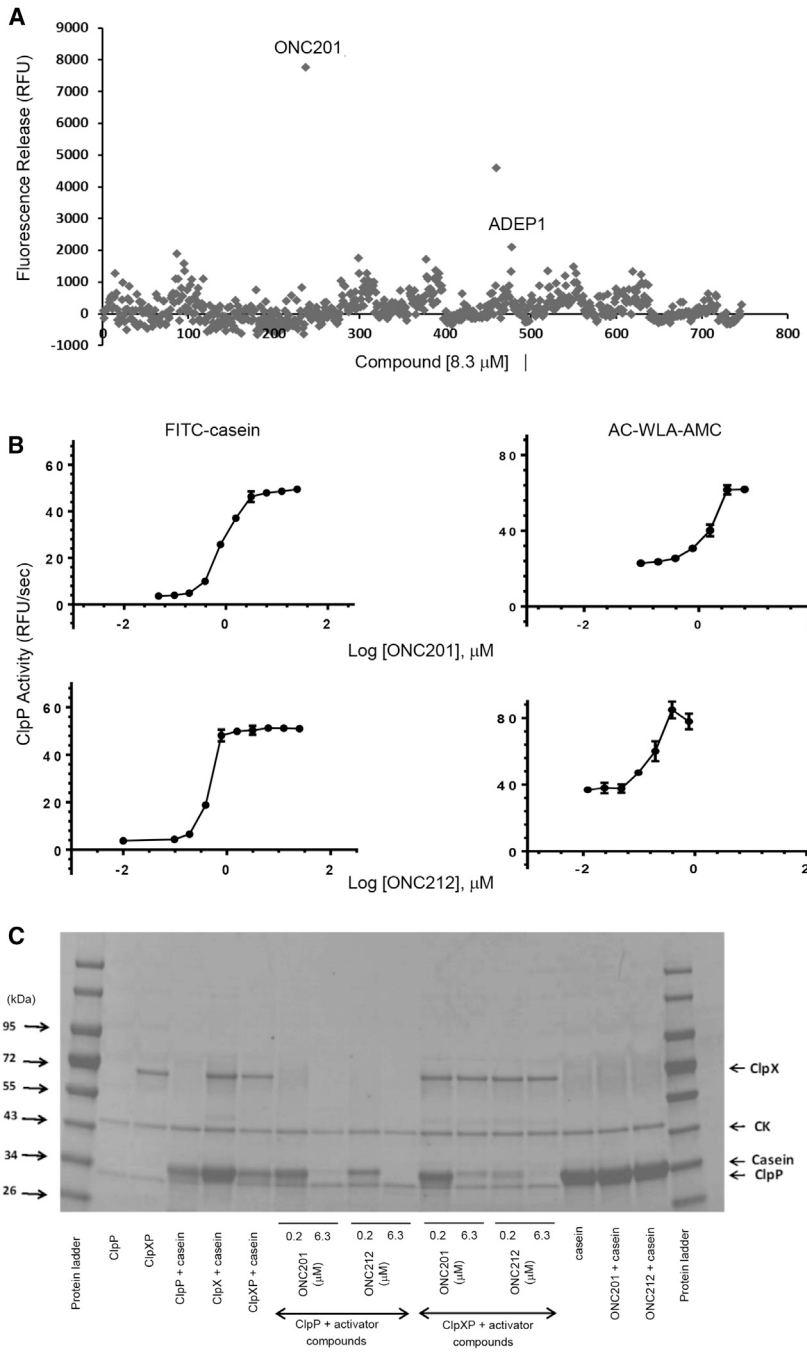

Figure 2. The Imipridones ONC201 and ONC212 Activate Mitochondrial ClpP

(A) Degradation rate of fluorogenic substrate FITC-casein by recombinant WT ClpP incubated with each compound of a chemical library of 747 molecules.

(B) Effects of ONC201 and ONC212 on degradation of fluorogenic substrates AC-WLA-AMC and FITC-casein by recombinant WT ClpP. The results are expressed as the mean value of triplicate samples ± SD (error bars).

(C) Degradation of α-casein by purified recombinant WT ClpP and ClpXP complexes treated for 3 h with ONC201, ONC212, or vehicle control (DMSO) in FITC-casein assay buffer detected on SDS-PAGE. See also Figure S2.

addition of ONC201 and ONC212 activated ClpP and induced cleavage of α-casein without the need for ClpX.

Taken together, we identified ONC201 and ONC212 as potent ClpP activators.

ONC201 Binds ClpP Non-covalently at the Interface with ClpX

We then investigated if imipridones interact with ClpP, and found that ONC201 directly interacted with the recombinant ClpP using isothermal titration calorimetry (ITC) by either titrating ONC201 to a solution of ClpP (Figure 3A) or titrating ClpP into a solution of ONC201 (Figures S3A and S3B) (Gersch et al., 2015). Using gel filtration (Figure S3C), we observed a clear shift of ClpP toward higher molecular weight in the presence of ONC201, thus confirming direct interaction of ONC201 with ClpP. As human mitochondrial ClpP was shown to exist as a heptamer in the absence of ClpX (Kang et al., 2005), even at concentrations >3 mg/mL, ONC201 binding to the protease appeared to shift the equilibrium from the 7-mer to the 14-mer of ClpP.

To identify the precise molecular interaction between ONC201 and ClpP, we co-crystallized human ClpP with ONC201 and determined the structure of the complex at 2 Å resolution (PDB: 6DL7). Seven ONC201 molecules are clearly visible in the electron density map (Figures 3B and S3D–S3F). They each occupy hydrophobic pockets between adjacent subunits. Binding between ClpP and ONC201 involves extensive hydrophobic contacts and a hydrogen bond to the hydroxyl group of Tyr-118 (2.8 Å). In addition, the oxo-group of ONC201 forms water-mediated hydrogen bonds with the side chain nitrogen of Gln-107 and the carbonyl oxygen of Leu-104. The phenyl ring of ONC201 is positioned between Tyr-138 and Tyr-118, engaging in π-stacking interactions.

The binding of ONC201 leads to the axial entrance pore opening up, increasing its radius from 12 Å, as in an apparently closed conformation of human mitochondrial ClpP (Kang et al., 2004), to 17 Å (Figure 3C, top). The ClpP 14-mer assumes a more compact form and its height decreases from 93 to 88 Å (Figure 3C, bottom). The N-terminal residues of ClpP show increased dynamics, demonstrated by their significantly higher temperature factors (Figure 3D). Electron density is very weak for the first 7 N-terminal residues and not observable at all for residues 64–73 and amino acids following Pro-248. ONC201 binding induces further structural changes around the active site region at the

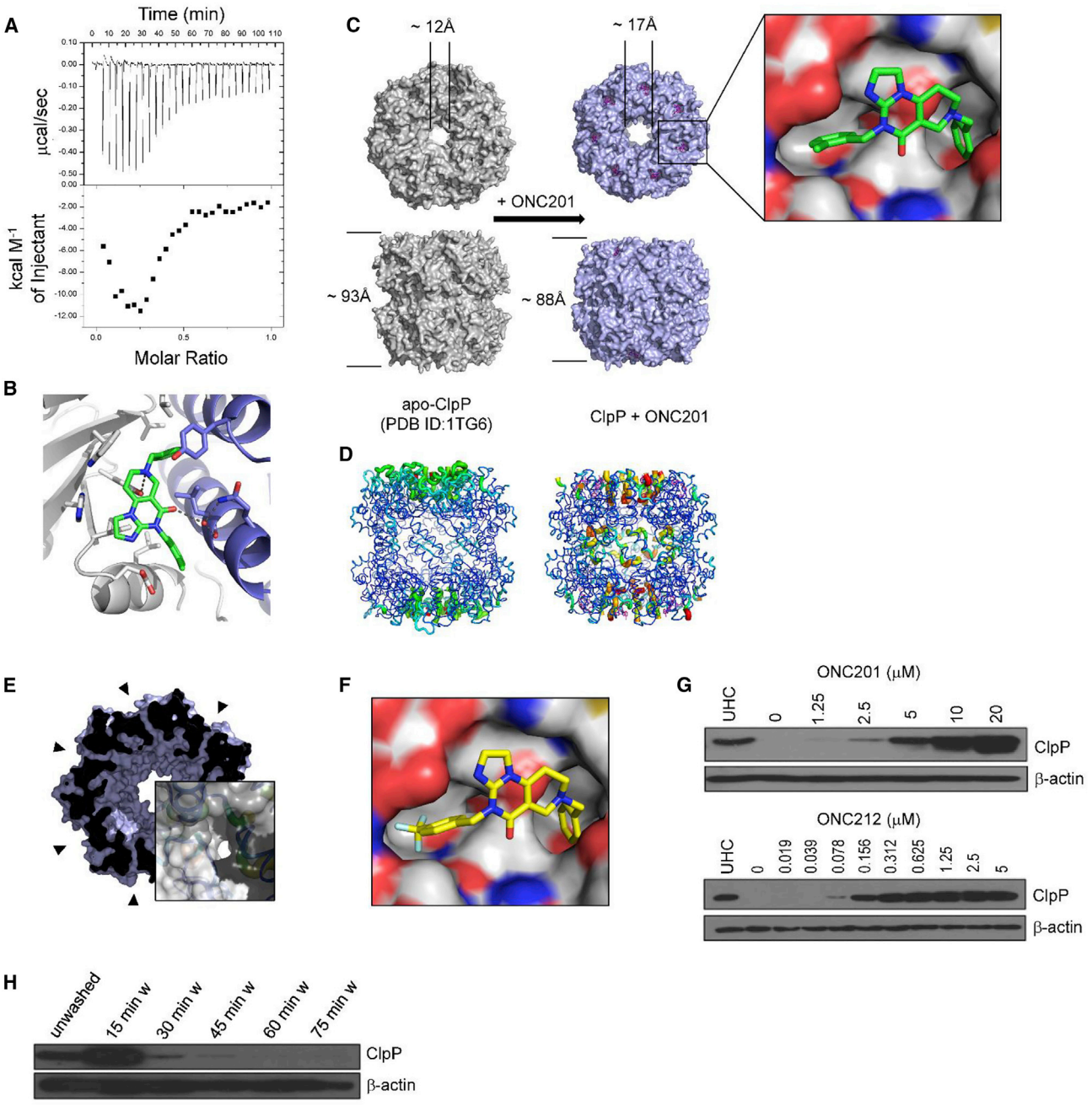

Figure 3. The Imipridones Bind to ClpP and Are Cytotoxic to Leukemia and Lymphoma Cells

(A) Isothermal calorimetry binding experiment of 100 µM ONC201 titrated into 20 µM ClpP (concentration of ClpP monomer).

(B) The co-crystallography result focusing on the hydrophobic pocket between two ClpP subunits bound to ONC201. Hydrogen bonds are indicated by dashed lines and water molecule-mediating hydrogen bonding as a red sphere.

(C) Top (top) and side (bottom) views of human apo-ClpP (gray; PDB: 1TG6) and its ONC201 complex (blue) in surface representation; the ONC201 molecule is shown in magenta. Insert: ONC201 molecule in stick representation against ClpP surface.

(D) Apo-ClpP (left) and its ONC201 complex (right) color-coded according to residue B factors (low to high, blue to red). Insert color coding: carbon in green (ligand) and white (protein), nitrogen in dark blue, oxygen in red.

(E) Cross-section through the human ONC201-complexed ClpP tetradecamer; positions of side pores are indicated by black triangles. Close-up of the pore (insert) between chains C (bottom left), D (bottom right), and symmetry-related chain K (top). Protein chains are indicated by ribbons colored based on residue B factors (blue to red, low to high; protein surface in shades of gray).

(F) Model of ONC212-binding to ClpP. The ligand is displayed as sticks and the surrounding protein is shown in surface representation. Color coding as in (C) but carbon in yellow (ligand); fluorine in light blue.

(legend continued on next page)

heptamer-heptamer interface. In the human apo-ClpP structure (Kang et al., 2004), this region is well defined. In the ClpP-ONC201 complex, residues 178–193, encompassing the end of strand β6, all of strand β7, and the first third of helix α5, undergo a large conformational change and show increased dynamics with the region around residues 183–187, again not visible in electron density maps (Figure 3D). This change directly impacts the placement of the catalytic triad residues (Ser-153, His-178, and Asp-227) in the active site. The His-178 ring separates from Ser-153 by more than 5 Å, while rotating by about 70°. Asp-227 moves 2.8 Å in the same direction (Figure S3F). Notably, in the ONC201 complex, the catalytic aspartates from subunits, which in the tetradecameric ring are located across from each other at the heptamer-heptamer interface, approach rather closely (4.6 Å), whereas they are separated by ca. 17 Å in the apo-structure. In addition, Ser-181 is now nearer to His-178 than the catalytic Ser-153, with the former's hydroxyl group 3.2 Å away from the neighboring subunit's Asp-227 carboxylate. Changes induced by ONC201-binding include the opening of channel-like pores in the central region of the "side wall" of the protease, similar to those described for the bacterial enzyme; they represent potential escape routes for peptide products (Sprangers et al., 2005) (Figure 3E).

In ONC212, the 4-(2-methylbenzyl) group of ONC201 is replaced by a 4-(4-trifluoromethylbenzyl). In the ClpP-ONC201 complex, the ortho-methyl group of ONC201 points toward bulk solvent. Its removal should be of minor influence on ONC201 binding. Fluorophilic environments in proteins include peptide bonds, especially in hydrophobic surroundings, engaging in C-F···H-N, C-F···C=O, and C-F···H-C_α multipolar interactions. Positively charged arginines can also contribute to binding enhancement (Müller et al., 2007). Modeled on the ONC201 complex and subjected to two cycles of molecular dynamics refinement (Adams et al., 2010), ONC212's p-CF_3-benzyl substituent extends into a generally apolar pocket of ClpP (Figure 3F). With atomic movements < 1 Å, no clashes with protein residues are seen. The peptide bonds of Ile-75, Leu-79, Ala-101, and Phe-105 are close enough to interact. The side chains of Arg-78 and Arg-81 can swing around and interact with the CF_3 substituent. Arg-81 can displace Arg-78 in its salt bridge with Glu-82; the three residues are on the protein surface and in contact with bulk solvent. The highly electronegative CF_3 substituent likely enhances ONC212's potency by providing more opportunities for multipolar bonds and an improved structural complementarity to ClpP.

We then tested whether ONC201 and ONC212 could bind ClpP in cells using a cellular thermal shift assay (CETSA). CETSA evaluates ligand-induced changes in melting temperature of target proteins in cells to determine the binding affinity of ligands toward their targets (Jafari et al., 2014). Both ONC201 and ONC212 bound endogenous ClpP in OCI-AML2 at concentrations associated with activation of the protease in the enzymatic assays (Figures 3G and S3G). We then tested the reversibility of binding of ONC201 to ClpP in OCI-AML2 cells by washing ONC201-treated cells in PBS and re-incubating them in fresh media before the CETSA assay (Figure 3H). ClpP thermal stability rapidly decreased following removal of drug from the media, consistent with non-covalent binding observed in the crystal structures.

ClpP Activation by Imipridones Kills Malignant Cells through a ClpP-Dependent Mechanism

We further evaluated the effects of hyperactivating ClpP on the growth and viability of cancer cells. Both ONC201 and ONC212 reduced the growth and viability of OCI-AML2, OCI-AML3, TEX leukemia cells, and Z138 lymphoma cells, as well as HCT-116 colon cancer, HeLa cervical cancer, OC316 ovarian cancer, and SUM159 breast cancer cells, with IC_{50} values in the low micromolar (ONC201) or nanomolar range (ONC212) (Figures 4A, S4A, and S4B). Moreover, ONC201 and ONC212 induced apoptosis in primary AML patient samples, including those with high-risk cytogenetics and molecular mutations, but had little effect on normal hematopoietic cells (Figure 4B; Table S1).

To assess whether activation of ClpP is functionally important for cell death induced by imipridones, we treated *CLPP*$^{+/+}$ and *CLPP*$^{-/-}$ T-REx HEK293 cells with increasing concentrations of ONC201, ONC201 inactive isomer, and ONC212. ONC201, and ONC212 reduced the growth and viability of *CLPP*$^{+/+}$, but not *CLPP*$^{-/-}$, cells (Figure 4C). ONC201 isomer did not significantly decrease the growth and viability of *CLPP*$^{+/+}$ or *CLPP*$^{-/-}$ T-REx HEK293, and ONC201-sensitive or ONC201-resistant Z138 cells (Figures S4C and S4D).

To identify whether ClpP expression levels in primary AML samples predict their response to ClpP activators, we measured pretreatment ClpP levels in 11 primary AML samples and assessed their response to ONC201 treatment. Sensitivity to ONC201 correlated with pretreatment ClpP expression in these samples (Figures 4D and S4E; Table S2). Primary AML patient samples with higher ClpP expression were statistically significantly more sensitive to the ClpP activator compared with samples with pretreatment ClpP values that were 1 SD below average (Figure 4E). Thus, ClpP activators preferentially induce cell death and apoptosis in primary AML over normal cells and ClpP expression might serve as a biomarker for patients who respond to ClpP activators, including ONC201 and ONC212.

Inactivating Mutations in ClpP Render Cells Resistant to Imipridones

To further evaluate the importance of ClpP for ONC201- and ONC212-mediated cell death and to identify potential mechanisms of resistance to ClpP activators, we treated Z138 cells with increasing concentrations of ONC201 and selected a population of cells resistant to it (ONC-R Z138). ONC-R Z138 cells were also cross-resistant to ONC212 (Figure 5A), but retained

(G) Concentration-dependent effects of treatment with ONC201 and ONC212 on thermal stability of endogenous ClpP in OCI-AML2 cells assessed using cellular thermal shift assays (CETSA). UHC, unheated control.

(H) Effect of ONC201 removal from media on thermal stability of endogenous ClpP in intact OCI-AML2 cells. ONC201 (10 μM)-treated cells were washed with PBS and re-incubated in fresh medium for up to 75 min before CETSA. w, wash.

See also Figure S3.

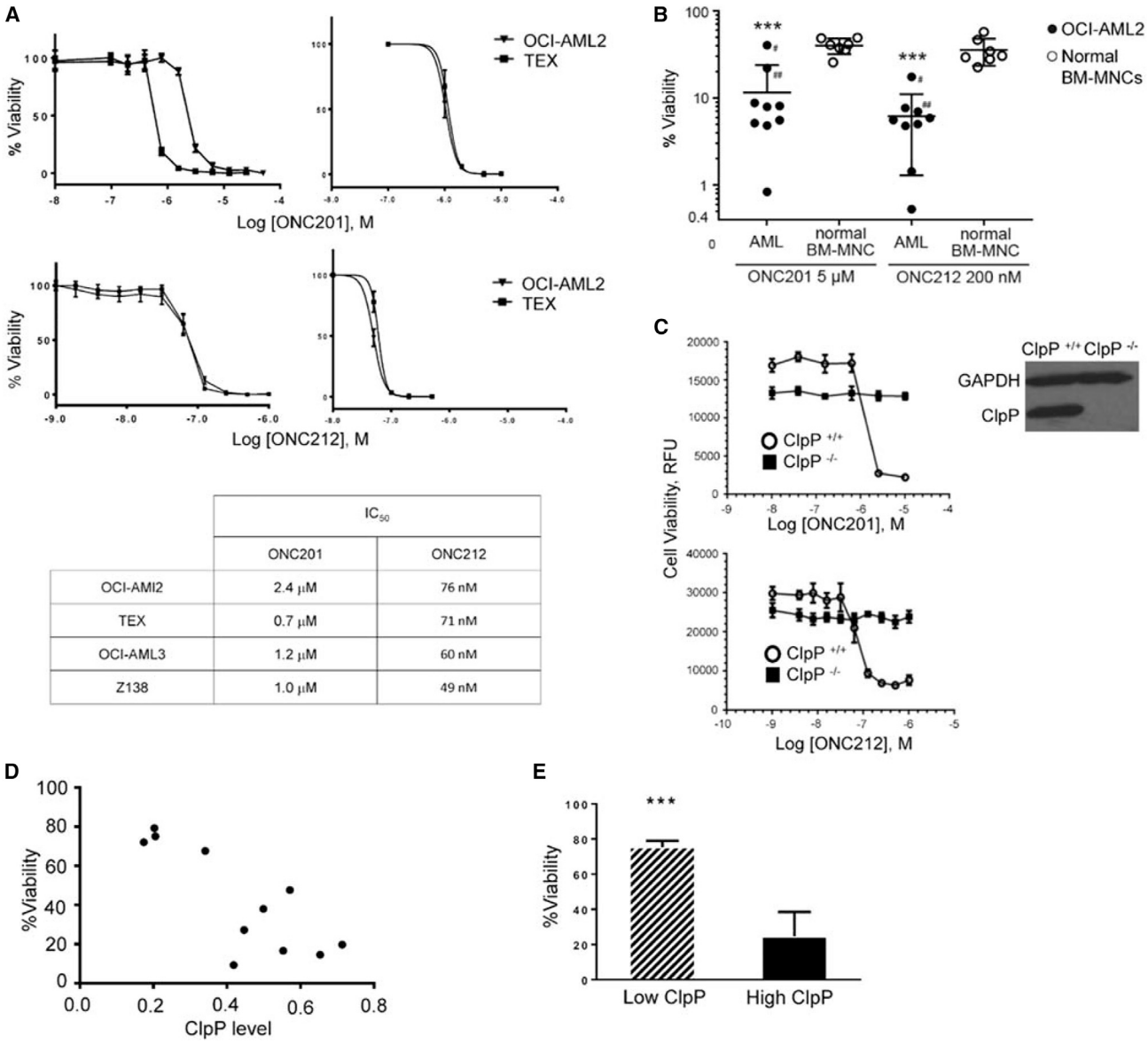

	IC_{50}	
	ONC201	ONC212
OCI-AMl2	2.4 μM	76 nM
TEX	0.7 μM	71 nM
OCI-AML3	1.2 μM	60 nM
Z138	1.0 μM	49 nM

Figure 4. ClpP Activation by Imipridones Kills Malignant Cells through a ClpP-Dependent Mechanism

(A) Effects of ONC201 and ONC212 on viability of OCI-AML2, TEX, OCI-AML3, and Z138 cells. Data represent percent mean ± SD viable cells measured by Alamar Blue assay in OCI-AML2, TEX cells, or by annexin V assay in OCI-AML3 and Z138 cells, after a 72-h period of exposure to the drugs.

(B) Changes in live cell number by ONC201 and ONC212 compared with untreated controls in primary AML and normal bone marrow mononuclear cells (BM-MNC). Cells were treated with ONC201 and ONC212 at indicated concentrations for 72 h. Annexin V- and DAPI-negative cells were measured by flow cytometry and normalized to that in untreated controls. Data represent mean ± SD. #, ##: samples that were relatively resistant to ONC201.

(C) Effects of ONC201 and ONC212 on the viability in $ClpP^{+/+}$ and $ClpP^{-/-}$ T-REx HEK293 cells and protein expression of ClpP. Data represent percent mean ± SD viable cells measured by Alamar Blue assay after a 72-h period of exposure to the drugs.

(D) Correlation between pretreatment expression level of ClpP and the effects of ONC201 on viability of primary AML samples measured by annexin V assay after a 72-h period of exposure to the drug (D). R = −0.82, p = 0.003. ClpP levels were quantified by immunoblot analysis of untreated samples.

(E) The correlation in (D) is plotted by dichotomizing the ClpP expression. Low ClpP, samples with ClpP levels that were 1 SD below average. High ClpP, all other samples. The results are expressed as the mean value of triplicate samples ± SD (error bars). ***p < 0.001.

See also Figure S4 and Tables S1 and S2.

similar sensitivity to adriamycin and vincristine (Figure S5A). Using RNA sequencing (RNA-seq) and unbiased analysis, we identified D190A mutation in ClpP (Figure S5B) with an allele frequency of 47% in the ONC-R Z138 cells. Sanger sequencing of genomic DNA confirmed the heterozygous D190A mutation in *CLPP* in all seven randomly-selected clones resistant to ONC201 and ONC212 (Figures S5C–S5E).

To assess how the D190A mutation affects ClpP function, we generated and purified recombinant D190A ClpP and measured its enzymatic activity and response to ONC201 and ONC212.

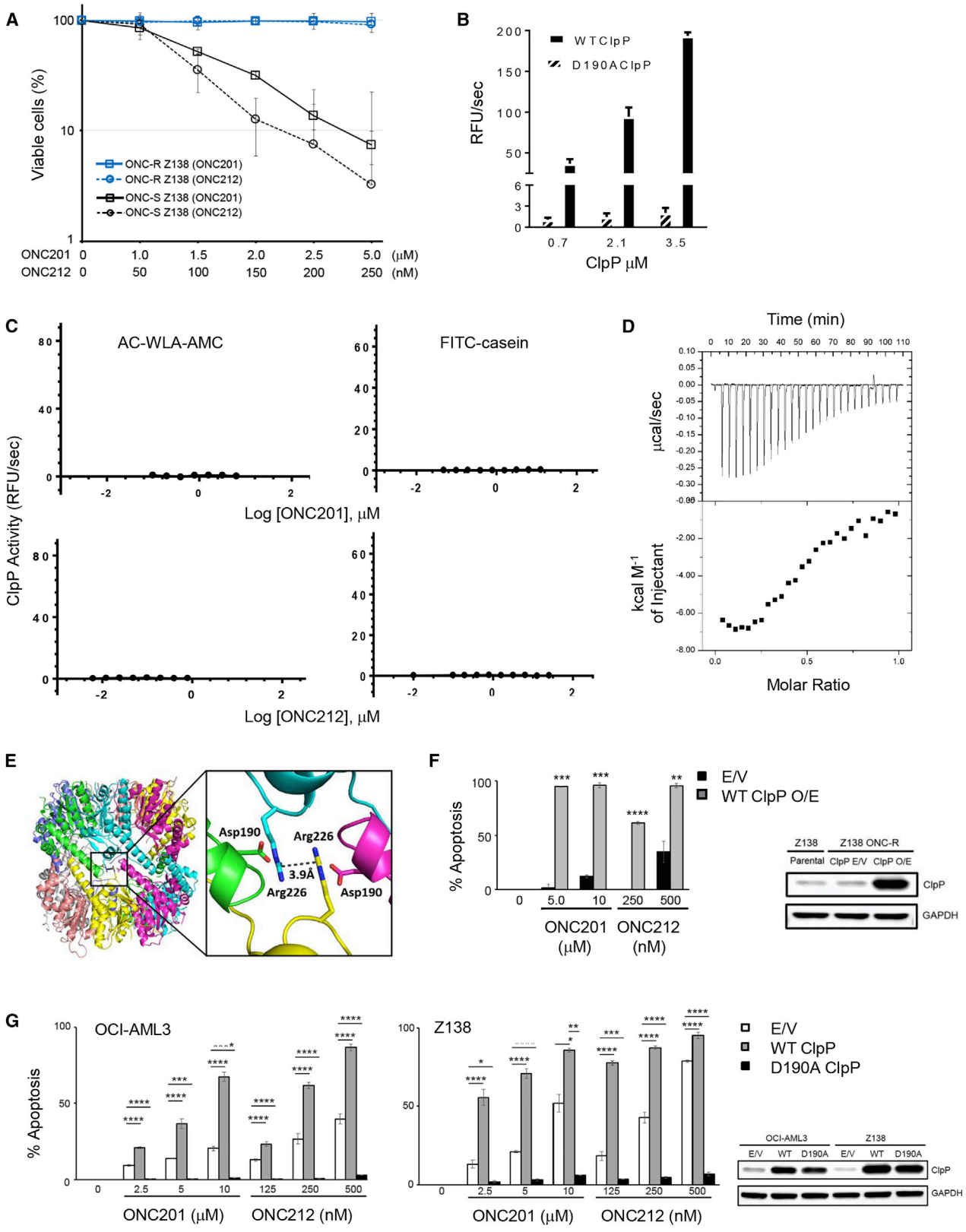

Figure 5. Cytotoxicity of Imipridones is ClpP Dependent

(A) Sensitivity of ONC201-sensitive and ONC201-resistant Z138 to ONC201 and ONC212 was assessed by annexin V assays. Data represent percent mean of triplicate samples ± SD (error bars) for viable (annexin V and propidium iodide double-negative) cells.

(legend continued on next page)

D190A ClpP had minimal proteolytic activity and could not degrade the fluorogenic peptide AC-WLA-AMC or FITC-casein under basal conditions (Figure 5B). Moreover, ONC201 and ONC212 could not activate proteolytic activity of D190A ClpP for either peptide or protein substrates (Figure 5C). However, ONC201 continued to bind recombinant D190A ClpP protease, as its binding site is a distance away from the mutation site, but the binding affinity was moderately reduced (Figure 5D).

To understand how the D190A mutation might affect ClpP activity and structure, we compared the apo-ClpP structure (Kang et al., 2004) with its ClpP-ONC201 complex. In the former, Asp-190 is located at the dimer interface and is important as a compensating charge to an unusual stacked arginine pair that consists of Arg-226 residues from two neighboring peptide chains (Figure 5E). Asp-190 is also only 6.4 Å from Asp-227 of the catalytic triad of ClpP (Figure S6A). However, in the ClpP-ONC201 complex structure this region undergoes a major conformational change and displays high mobility with Asp-190 in close proximity to Asp-93 in most subunits. Loss of negative charge in D190A mutant can therefore have deleterious effects on the active site through impacting the mobility and side chain interactions of the 178–193 loop.

To determine whether the D190A mutation was functionally important for resistance to ONC201 and ONC212, we overexpressed the WT ClpP in ONC-R Z138 cells and overexpressed the D190A mutant ClpP in parental Z138, OCI-AML3, and HCT116 cells. Overexpression of WT ClpP restored the sensitivity to ONC201 and ONC212 to ONC-R Z138 cells (Figures 5F and S6B), while overexpression of D190A ClpP in parental Z138, OCI-AML3, and HCT116 cells made them resistant to ONC201 and ONC212 (Figures 5G, S6C, and S6D). Of note, overexpression of WT ClpP in parental Z138 and OCI-AML3 cell lines increased sensitivity to ONC201 and ONC212 (Figure 5G). Thus, these data suggest that activation of ClpP is functionally important for cell death induced by ONC201 and ONC212 and identify a mechanism of resistance to ClpP activators.

ClpP Activation Leads to Reduction in Respiratory Chain Complex Subunits and Impaired Oxidative Phosphorylation

We next used BioID (Roux et al., 2012) to identify interacting partners of ClpP after chemical or genetic activation. To chemically hyperactivate the protease, T-REx HEK293 cells expressing FlagBirA-ClpP(WT) were treated with 0.6 μM ONC201 for 48 h. As a genetic approach, we expressed FlagBirA-ClpP (Y118A). We compared the interactome of activated ClpP to non-stimulated WT ClpP. Proteins that interacted with unstimulated WT ClpP in the BioID assay but whose spectral counts decreased when ClpP was activated were postulated to represent potential substrates of hyperactivated ClpP.

Over 200 mitochondrial proteins were identified as high-confidence ClpP interacting partners. Of these polypeptides, 90 displayed a $\geq$ 4-fold decrease in spectral counts ($p \leq 0.001$) following ONC201 treatment. Among the proteins displaying the most robust decrease were components of the electron transport chain (and in particular, subunits of respiratory chain complex I) and polypeptides involved in mitochondrial translation (Figure 6A; Table S3). Expression of the constitutively active Y118A ClpP mutant yielded a depletion of an overlapping set of interacting partners, but the degree of reduction in peptide counts was smaller than that observed in response to ONC201, likely reflecting the weaker activation of the protease by the mutation (Table S3).

Respiratory chain subunits SDHA and SDHB had previously been identified as putative ClpP substrates and inhibition of ClpP led to the accumulation of degraded or misfolded subunits (Cole et al., 2015). To investigate the effects of ClpP activation on the levels of proteins identified as interacting partners in our BioID assay, we treated Z138 cells with ONC201 and found that such treatment decreased levels of respiratory chain complex proteins, with the reduction of the respiratory chain I subunit NDUFA12 being most pronounced (Figure 6B). In contrast, levels of these proteins did not markedly change after treating ONC-R Z138 cells with ONC201, overexpressing WT ClpP restored the ability of ONC201 to reduce respiratory chain complex proteins in these cells (Figure 6B). Finally, overexpressing D190A mutant ClpP in WT Z138 cells rendered respiratory chain proteins resistant to ONC201-induced reduction (Figure 6C). ONC212 reduced the level of the identified ClpP interactors in a dose-dependent manner (Figures S7A and S7B). The reduction in NDUFA12 and SDHB by ONC212 was also observed in other cells (Figure S7C), which was blocked by overexpression of the D190A ClpP mutant (Figure S7D). Although we observed reductions in respiratory chain proteins, levels of mRNA encoding these substrates were either unchanged or increased (Figure S7E). Furthermore, the addition of recombinant ClpP and ONC201 to lysates of mitochondria isolated from *CLPP*$^{-/-}$ HEK293T-REx and OCI-AML2 cells decreased levels of the complex I subunit NDUFB8 and complex III subunit UQCRC2, indicating that ClpP activation can increase the degradation of selective ClpP substrates, independent of cytoplasmic or nuclear pathways (Figure S7F). Likewise, expression of the Y118A ClpP mutant led to reductions in SDHA, SDHB, and

(B) Effects of WT and D190A-ClpP on degradation of fluorogenic AC-WLA-AMC. The results are expressed as the mean value of triplicate samples ± SD (error bars).
(C) Effects of ONC201 and ONC212 on degradation of the fluorogenic substrates AC-WLA-AMC and FITC-casein by D190A ClpP. The results are expressed as the mean value of triplicate samples ± SD (error bars).
(D) ITC data for ONC201 (100 μM) titrated into D190A-ClpP (20 μM; concentration of ClpP monomer).
(E) The location of D190 and R226 at the interface of two heptamer rings in an apparently closed conformation of human mitochondrial ClpP.
(F) Apoptosis induction by imipridones when WT ClpP is overexpressed (O/E) in ONC-R Z138 cells carrying D190A mutant ClpP. Cells were treated with ONC201 and ONC212 at the indicated concentrations for 72 h. E/V, empty vector as control. Protein expression levels of ClpP was assessed by immunoblotting.
(G) Apoptosis induction by imipridones when WT or D190A-ClpP is overexpressed (O/E) in parental Z138 and OCI-AML3 cells. Cells were treated with ONC201 and ONC212 at the indicated concentrations for 72 h. Protein expression levels of ClpP were assessed by immunoblotting. The results are expressed as the mean value of triplicate samples ± SD (error bars) for annexin V-positive cells. *$p < 0.05$, **$p < 0.01$, ***$p < 0.001$, ****$p < 0.0001$ (F and G).
See also Figures S5 and S6.

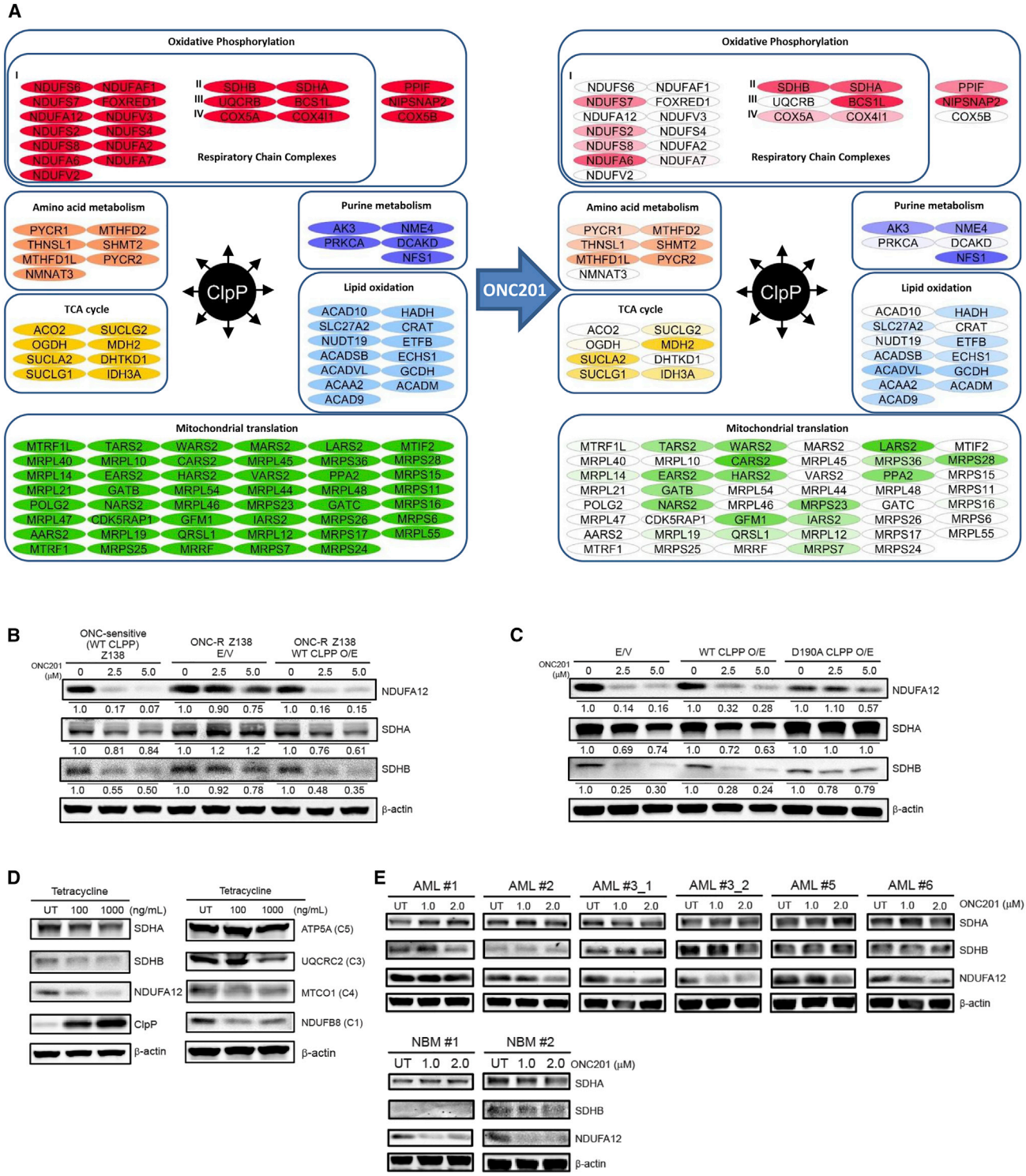

Figure 6. ClpP Hyperactivation Induces Apoptosis Following Reduction of Respiratory Chain Complex Subunits

(A) A subset of ClpP mitochondrial interactors was identified using BioID-MS and categorized according to selected gene ontology biological processes. Decreases in spectral counts following ONC201 treatment are illustrated and proportional to the decreases in color intensity.

(B–E) Immunoblot analysis of respiratory chain complex subunits in parental (ONC-sensitive) Z138 cells and ONC-R Z138 cells (clone no. 2) with overexpression of WT ClpP or an empty vector (B); in parental Z138 cells with overexpression of WT ClpP, D190A mutant ClpP, or an empty vector (C); in Z138 cells with tetracycline-inducible Y118A mutant ClpP (D); and in primary AML cells and normal bone marrow (NBM) cells (E). AML no. 3_1 and no. 3_2 are from the same patient, but at different time points in relapse. Cells were treated with ONC201 at indicated concentrations for 24 h.

See also Figure S7 and Table S3.

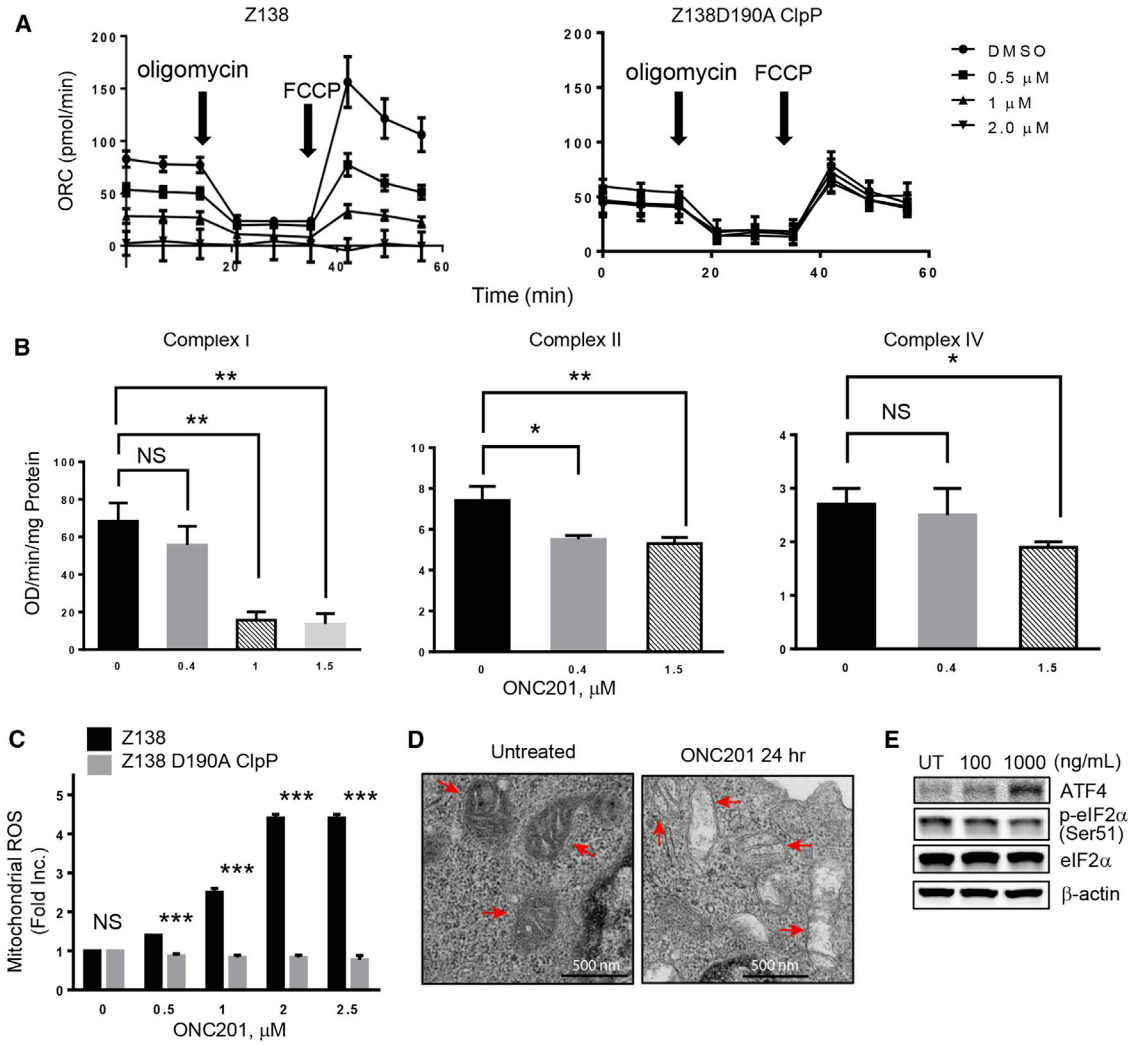

Figure 7. ClpP Hyperactivation by ONC201 Impairs Oxidative Phosphorylation

(A) Effect of ONC201 on oxygen consumption rate (OCR) per 1 × 10^5 cells in Z138 and Z138 D190A ClpP cells (measured by Seahorse Analyzer). The results are expressed as the mean value of triplicate samples ± SD (error bars).

(B) Effects of ONC201 treatment on activity of respiratory chain complexes I, II, and IV in OCI-AML2 cells. The results are expressed as the mean value of triplicate samples ± SD (error bars). *$p < 0.05$, **$p < 0.01$.

(C) Effect of ONC201 treatment on mitochondrial reactive oxygen species (ROS) production in Z138 and Z138 D190A ClpP cells. The results are expressed as the mean value of triplicate samples ± SD (error bars). ***$p < 0.001$.

(D) A transmission electron microscopy image of mitochondria in OCI-AML3 cells treated with or without 5 μM ONC201 for 24 h.

(E) Immunoblot of ATF4, p-eIF2α and eIF2α in Z138 cells with tetracycline-inducible Y118A ClpP treated with tetracycline for 48 h at the indicated concentrations.

NDUFA12 in a dose-dependent manner (Figure 6D). In contrast, another respiratory complex subunit, ATP5A, was not reduced by Y118A ClpP overexpression, ONC201 or ONC212 (Figures 6D and S7B), reflecting selective degradation of particular subunits by ClpP activation.

We also tested the effects of ONC201 and ONC212 on levels of respiratory chain proteins in primary AML cells and observed a reduction in respiratory chain proteins (Figure 6E). Interestingly, imipridone treatment similarly reduced respiratory chain proteins in normal hematopoietic cells (Figure 6E). Thus, greater sensitivity of AML cells to ClpP activation likely reflects their increased reliance on oxidative phosphorylation and lower spare reserve capacity in their respiratory chain (Sriskanthadevan et al., 2015).

Next, we investigated the effects of ClpP activation on oxidative phosphorylation and mitochondrial function. Treatment with ONC201 decreased basal oxygen consumption rate and spare reserve capacity in Z138 cells with WT ClpP but not in Z138 cells with D190A ClpP (Figure 7A). Likewise, ClpP activation decreased the enzymatic activity of respiratory chain complexes I, II, and IV, with complex I being the most sensitive (Figure 7B). Finally, ClpP activation increased the production of mitochondrial reactive oxygen species in Z138 cells with WT ClpP, but not in Z138 cells with D190A ClpP (Figure 7C). Consistently, mitochondria were morphologically damaged by ONC201 treatment, as assessed by electron microscopy, demonstrating particular damages of matrix and cristae structures (Figure 7D).

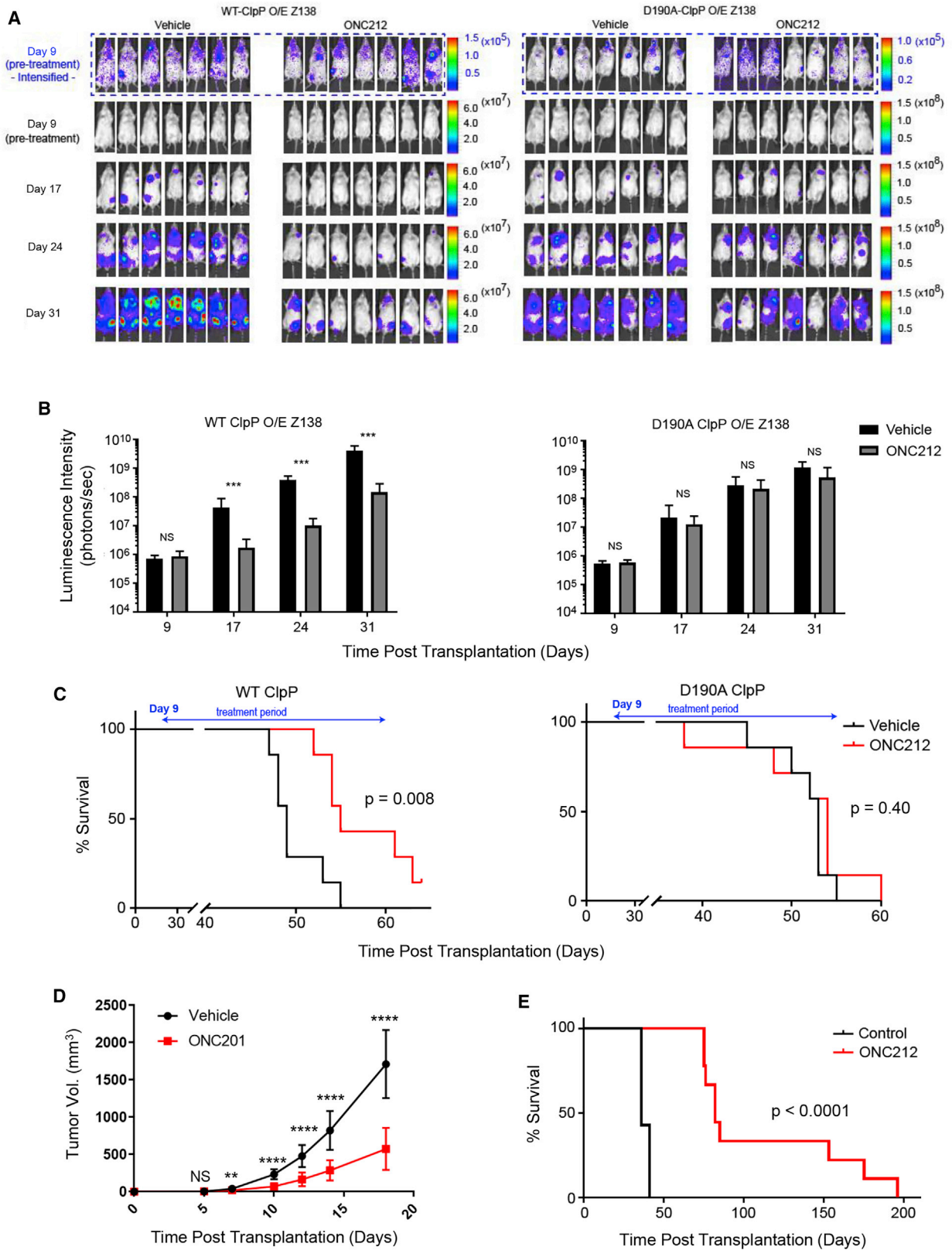

(legend on next page)

We previously reported that ONC201 induces atypical integrated stress response (ISR) where ATF4 protein increase is induced irrespectively of phosphorylation status of eIF2α, unlike classical ISRs (Ishizawa et al., 2016). Indeed, overexpression of Y118A ClpP in Z138 cells showed increase in ATF4 protein without increasing phosphorylation of eIF2α (Figure 7E).

ClpP Activation by Imipridones Exerts Anti-tumor Effects *In Vivo*

To test if ClpP activation by ONC212 induces anti-tumor effects *in vivo*, we established xenograft mouse models using Z138 cells with WT or D190A ClpP overexpression and treated the mice with oral gavage of ONC212. The Z138 cells were luciferase labeled, and systemic tumor burden was followed by measuring luciferase activity with IVIS imaging. Consistent with our *in vitro* anti-cancer findings, tumor burden was significantly reduced by ONC212 treatment in the WT ClpP group, whereas there was no discernable anti-tumor activity in the D190A ClpP group (Figures 8A and 8B). Animal survival was significantly prolonged in the ONC212-treated WT ClpP group, but not in the D190A mutant group (median survival: WT, 49 versus 55 days; D190A mutant, 53 versus 54 days) (Figure 8C). The result suggested that *in vivo* efficacy of ONC212 is ClpP dependent. We also validated the *in vivo* anti-tumor effects of ONC201 in a xenograft model of OCI-AML2 cells. Oral ONC201 significantly reduced the leukemic burden in mice compared with the control group (Figure 8D). Collectively, imipridones are effective *in vivo* in lymphoma and AML mouse models. To further evaluate the effects of ONC212 on leukemia-initiating cells (LICs), we treated patient-derived xenograft AML cells from secondarily engrafted mice (i.e., LICs enriched) with ONC212, and then injected the cells into recipient NSG mice. Survival of the mice was significantly prolonged (median survival: 36 versus 82 days) (Figure 8E), suggesting that ClpP activation inhibits the engraftment capacity of LICs. In an ongoing clinical trial in patients with relapsed/refractory AML, decrease in circulating blasts and subsequent increase in platelet counts was observed (Figure S8) following a single dose of ONC201 (250 mg orally).

DISCUSSION

Despite recently developed targeted agents, most hematologic malignancies and solid tumors are incurable. This includes essentially all tumors with *TP53* mutations. Therefore, anti-tumor agents with unique mechanisms of action are urgently needed. Accumulating evidence demonstrates that mitochondrial function is critical for maintenance and therapy resistance of leukemias (Cole et al., 2015; Farge et al., 2017; Kuntz et al., 2017; Moschoi et al., 2016; Samudio et al., 2010; Skrtic et al., 2011) and certain solid tumors (Birsoy et al., 2014; Kotschy et al., 2016; Viale et al., 2014), and therapeutic strategies to effectively disrupt the integrity of mitochondria have been investigated (Birsoy et al., 2014; Cole et al., 2015; Konopleva et al., 2006, 2016; Kotschy et al., 2016; Kuntz et al., 2017; Pan et al., 2014, 2017; Skrtic et al., 2011; Viale et al., 2014). Here we found that ClpP hyperactivation induces lethality in leukemias and lymphomas, owing to selective proteolysis of subsets of the mitochondrial proteome that are involved in mitochondrial respiration and oxidative phosphorylation. Our findings also provide an explanation for the recent report demonstrating that ONC201 reduces oxidative phosphorylation (Greer et al., 2018). Considering several recent reports showing that cancer stem and chemo-resistant cells rely highly on oxidative phosphorylation (Farge et al., 2017; Kuntz et al., 2017; Lagadinou et al., 2013; Marin-Valencia et al., 2012; Viale et al., 2014), we speculate that this therapeutic approach may also have potential to eliminate chemo-resistant populations of malignant cells and prevent relapse of the disease, which is an important direction to be addressed in future studies.

Deletions or mutations of ClpP have not been reported in primary AML, suggesting that ClpP could be an effective target across the spectrum of molecular and cytogenetic subsets of AML. However, our data suggest that patient samples with the lowest levels of ClpP are less sensitive to ClpP hyperactivation. Thus, levels of ClpP could serve as a biomarker to select AML patients most and least likely to respond to this therapy. Further studies with larger numbers of patients would be required to establish thresholds of ClpP expression that best predict response.

We established genetic systems to activate and inactivate human ClpP by identifying certain point mutations. We demonstrated that Y118A mutation in human ClpP leads to constitutive activation of the protease. We demonstrated that the D190A mutation we discovered in ONC201-resistant cells to be an inactivating mutation. Thus, we identified a potential mechanism of resistance to ClpP activators and established a system with which to study the biological role of ClpP and its activators.

Our screen identified agonists of mitochondrial ClpP that are more potent than ADEPs. ONC201 and ONC212 are a class of anti-cancer compounds that effectively kill cancer cells, but are much less toxic to normal cells (Allen et al., 2013; Ishizawa et al., 2016). Their efficacy is independent of *TP53* mutation status (Allen et al., 2013; Ishizawa et al., 2016). Although the preclinical efficacy of these compounds has been established in numerous cancers, the direct target was elusive. The dopamine receptor DRD2 has been suggested as a putative target of

Figure 8. ClpP Activation Exerts Anti-tumor Effects *In Vivo*

(A) Tumor burden measured by luciferase activity using IVIS imaging in xenograft mice with WT or D190A-mutant ClpP overexpressing Z138 cells treated with ONC212 (50 mg/kg every other day, oral gavage) or vehicle (n = 7 each) after confirming engraftment. Color scale bars represent relative luminescence intensity (photons/s).

(B) Intensities of luminescence detected by IVIS imaging in the mice in Figure 6A. The results are expressed as the mean value of triplicate samples ± SD (error bars). ***$p < 0.001$.

(C) Survivals of xenograft mice using Z138 cells overexpressed with WT or D190A ClpP.

(D) Tumor volumes of xenograft mice using OCI-AML2 cells treated with ONC201 (100 mg/kg twice daily, oral gavage) or vehicle (n = 10 each) from 5 days after transplantation for 13 days. The results are expressed as the mean value of n = 10 ± SD (error bars). **$p < 0.01$, ***$p < 0.001$.

(E) Survivals of NSG mice injected with PDX cells (t(9; 11) (p22; q23), *CEBPA* and *ATM* mutants) treated with or without 250 nM ONC212 for 36 h (n = 10 each). See also Figure S8.

ONC201 (Kline et al., 2016, 2018). However, DRD2 KO cells can be sensitive to ONC201 (Kline et al., 2018), suggesting that it may not be the functionally critical mechanism of action. Our crystal structure of the ClpP-ONC201 complex confirmed ClpP as a direct target for ONC201, and identified its binding pocket outside the active site. ONC201-mediated activation of ClpP has global structural effects that go beyond those of ADEP-mediated activation (Gersch et al., 2015; Lee et al., 2010). Drug binding not only stabilized the 14-mer but also widened the axial entrance pore and opened up channel-like pores on the side wall of the assembled protease. The increased opening, together with the increased dynamics of this region, suggests that these pores could provide a convenient escape route for cleaved peptide products. ONC201 binding not only increases the dynamics of the ClpP N-terminal residues, a region well known as a major regulatory site crucial for ClpX-mediated activation (Kang et al., 2004), but also induces major conformational changes at the heptamer-heptamer interface with direct effects on the active site region. ADEPs structural effects of activation of bacterial ClpP are most pronounced in the apical region of the protein with the heptamer-heptamer interface largely undisturbed (Gersch et al., 2015; Lee et al., 2010). A refined model of the ClpP-ONC212 complex suggests that its trifluoromethyl substituent enhances ONC212's potency through increased binding affinity and improved structural complementarity to ClpP.

We demonstrated that genetic ClpP activation results in ATF4 increase without increase in phosphorylated eIF2α in Z138 cells, validating our recent finding that ONC201 induces atypical ISR, which is characterized by eIF2α-independent induction of ATF4, unlike eIF2α-dependent classical ISRs (Ishizawa et al., 2016). This is also consistent with another recent report of eIF2α-independent ATF4 induction being downstream of mitochondrial unfolded stress response (UPR^{mt}) (Munch and Harper, 2016), and reflecting that activation of human ClpP phenocopies UPR^{mt}. Unlike ClpP functionality reported in *C. elegans* (Haynes et al., 2007; Quiros et al., 2016), several reports suggest that ClpP may not be a master regulator of UPR^{mt} in mammals (Bezawork-Geleta et al., 2015; Jin and Youle, 2013; Seiferling et al., 2016). Also, several reports indicate that UPR^{mt} may increase ClpP expression (Houtkooper et al., 2013; Zhao et al., 2002). However, it remains unknown how hyperactivating ClpP will affect UPR^{mt} signaling.

ONC201 is currently in early-phase clinical trials against AML and other cancers (Arrillaga-Romany et al., 2017; Kline et al., 2016; Stein et al., 2017), without serious adverse events reported yet. Thus, our findings related to ONC201 as a ClpP activator can immediately be validated in ongoing clinical trials in patients, and potentially also be tested in future clinical trials of its improved analogs, which include ONC206 (Wagner et al., 2017) and ONC212. Moreover, in conjunction with previous reports showing that ADEPs are promising antibiotics and that ADEP-resistant strains of staphylococcal isolates are rare (Conlon et al., 2013), imipridones may even exert effective antibiotic properties.

Of note, neither patients with Perrault syndrome, who carry inactivating mutations of ClpP, nor ClpP-deficient mice develop tumors. Previously, we demonstrated that inhibiting ClpP in leukemic cells leads to the accumulation of misfolded or damaged respiratory chain complex subunits that impair respiratory chain activity and causes cell death. In contrast, in our present study we showed that hyperactivating ClpP in cancer cells increases degradation of respiratory chain complex subunits leading to impaired respiratory chain activity. Thus, ClpP needs to be tightly regulated in malignancies as both inhibition and hyperactivation of ClpP impairs respiratory chain activity and causes cell death, although through different mechanisms.

In conclusion, hyperactivation of ClpP, which induces selective proteolysis of particular subsets of mitochondrial matrix proteins, is a potential therapeutic strategy against hematologic and solid tumors. Imipridones are currently being evaluated in clinical trials activators of ClpP other than imipridones could be developed in the future.

STAR★METHODS

Detailed methods are provided in the online version of this paper and include the following:

- KEY RESOURCES TABLE
- CONTACT FOR REAGENT AND RESOURCE SHARING
- EXPERIMENTAL MODEL AND SUBJECT DETAILS
  - Mice
  - Human Subjects and Primary Samples
  - Bacterial Cell Culture
- METHOD DETAILS
  - Protein Purification and Crystallization
  - Collection and Processing of Diffraction Data
  - Structure Solution and Refinement
  - Chemical Screen
  - ClpP Enzymatic Assays
  - Isothermal Titration Calorimetry (ITC)
  - Gel Filtration
  - Cell Culture
  - Cell Viability Assays
  - Cellular Thermal Shift Assay (CETSA)
  - RNA-Sequencing
  - Site Directed Mutagenesis
  - Immunoblot Analysis
  - Proximity-Dependent Biotin Labeling (BioID)
  - Mass Spectrometry Analysis
  - Network Analysis
  - Lentiviral Infection and ClpP Over-expression
  - Measurement of Oxygen Consumption Rate
  - Respiratory Chain Complexes Activity
  - Mitochondrial ROS Measurement
- QUANTIFICATION AND STATISTICAL ANALYSIS
- DATA AND SOFTWARE AVAILABILITY

SUPPLEMENTAL INFORMATION

Supplemental Information can be found online at https://doi.org/10.1016/j.ccell.2019.03.014.

ACKNOWLEDGMENTS

We thank Ronald A. DePinho for reviewing the manuscript; Rodrigo Jacamo, Teresa McQueen, and Venkata Lokesh Battula for support in establishing some of the engineered cell lines; Xiaoming Wang, Hong Mu, Huaxian Ma, Bing Carter, Qi Zhang, Lina Han, and Marina Konopleva for assisting in *in vivo*

studies; Jairo Matthews, Gheath Al-Atrash, and Steven Kornblau for primary sample and data collection, Wolfgang Oster at Oncoceutics for providing imipridones, and Shaun Labiuk, Canadian Light Source, for diffraction data collection. Part of the experiments were performed at the Sequencing and Microarray Facility, High Resolution Electron Microscopy Facility, and Flow Cytometry and Cellular Imaging Facility at MD Anderson, supported by CCSG grant NIH P30CA016672. This work was supported by the Canada Research Chairs program (to E.F.P.), Leukemia and Lymphoma Society, Canadian Institutes of Health Research, MaRS Innovation, the Ontario Institute for Cancer Research with funding provided by the Ontario Ministry of Research and Innovation, the Princess Margaret Cancer Centre Foundation, and the Ministry of Long Term Health and Planning in the Province of Ontario, the Barbara Baker Chair in Leukemia and Related Diseases (to A.D.S.); Haas Chair in Genetics, NIH Leukemia SPORE grant P50CA100632 and the University of Texas MD Anderson Cancer Center Support Grant CA016672, MDS/AML Moon Shot (to M.A.); and NIH Leukemia SPORE Career Enhancement Programs (to J.I.).

AUTHORS CONTRIBUTIONS

J.I., S.F.Z., A.D.S., and M.A. designed the study, analyzed results, and wrote the manuscript. R.E.D., W.M., and J.M.C.M. analyzed RNA-seq data. O.H. and E.F.P. designed and performed crystallography, modeling, ITC, gel filtration experiments and analyzed results and wrote the manuscript. J.S.T. analyzed the data and wrote the manuscript. R.Z., Y.J., L.E.H., J.S.T., V.R.R., T.N., G.E., S.H.B., Y.N., R.H., M.G., K.W., M.M., K.K., N.M., and A.B.L. performed the experiments and analyzed the data. T.L., G.B., and H.K. did study design, data analysis, and interpretation. M.D.M. provided critical reagents and supervised research. W.H. and B.R. supervised research and wrote the manuscript. M.S. designed the ONC212 chemical structure. R.E.D. and O.H. contributed equally to the study.

DECLARATION OF INTERESTS

M.S. is an employee and stockholder of Oncoceutics. M.A. serves on the scientific advisory board and is a stockholder of Oncoceutics. A.D.S. has received consulting fees from Novartis, Jazz and Otsuka Pharmaceuticals, and research grants from Medivir and Takeda Pharmaceuticals, and holds stock in Abbvie, Adamas Pharmaceuticals, Insmed, Myovant Sciences, Theravance Biopharma. We have filed invention disclosure forms related to the use of ONC201 in AML with high ClpP expression.

Received: September 4, 2018
Revised: November 13, 2018
Accepted: March 29, 2019
Published: May 2, 2019

REFERENCES

Adams, P.D., Afonine, P.V., Bunkoczi, G., Chen, V.B., Davis, I.W., Echols, N., Headd, J.J., Hung, L.W., Kapral, G.J., Grosse-Kunstleve, R.W., et al. (2010). PHENIX: a comprehensive Python-based system for macromolecular structure solution. Acta Crystallogr. D Biol. Crystallogr. *66*, 213–221.

Afonine, P.V., and Adams, P.D. (2012). On the contribution of hydrogen atoms to X-ray scattering. Comput. Crystallograph. Newslett. *3*, 18–21.

Allen, J.E., Kline, C.L., Prabhu, V.V., Wagner, J., Ishizawa, J., Madhukar, N., Lev, A., Baumeister, M., Zhou, L., Lulla, A., et al. (2016). Discovery and clinical introduction of first-in-class imipridone ONC201. Oncotarget *7*, 74380–74392.

Allen, J.E., Krigsfeld, G., Mayes, P.A., Patel, L., Dicker, D.T., Patel, A.S., Dolloff, N.G., Messaris, E., Scata, K.A., Wang, W., et al. (2013). Dual inactivation of Akt and ERK by TIC10 signals Foxo3a nuclear translocation, TRAIL gene induction, and potent antitumor effects. Sci. Trans. Med. *5*, 171ra117.

Arrillaga-Romany, I., Chi, A.S., Allen, J.E., Oster, W., Wen, P.Y., and Batchelor, T.T. (2017). A phase 2 study of the first imipridone ONC201, a selective DRD2 antagonist for oncology, administered every three weeks in recurrent glioblastoma. Oncotarget *8*, 79298–79304.

Bezawork-Geleta, A., Brodie, E.J., Dougan, D.A., and Truscott, K.N. (2015). LON is the master protease that protects against protein aggregation in human mitochondria through direct degradation of misfolded proteins. Sci. Rep. *5*, 17397.

Birsoy, K., Possemato, R., Lorbeer, F.K., Bayraktar, E.C., Thiru, P., Yucel, B., Wang, T., Chen, W.W., Clish, C.B., and Sabatini, D.M. (2014). Metabolic determinants of cancer cell sensitivity to glucose limitation and biguanides. Nature *508*, 108–112.

Brotz-Oesterhelt, H., Beyer, D., Kroll, H.P., Endermann, R., Ladel, C., Schroeder, W., Hinzen, B., Raddatz, S., Paulsen, H., Henninger, K., et al. (2005). Dysregulation of bacterial proteolytic machinery by a new class of antibiotics. Nat. Med. *11*, 1082–1087.

Cole, A., Wang, Z., Coyaud, E., Voisin, V., Gronda, M., Jitkova, Y., Mattson, R., Hurren, R., Babovic, S., Maclean, N., et al. (2015). Inhibition of the mitochondrial protease ClpP as a therapeutic strategy for human acute myeloid leukemia. Cancer Cell *27*, 864–876.

Conlon, B.P., Nakayasu, E.S., Fleck, L.E., LaFleur, M.D., Isabella, V.M., Coleman, K., Leonard, S.N., Smith, R.D., Adkins, J.N., and Lewis, K. (2013). Activated ClpP kills persisters and eradicates a chronic biofilm infection. Nature *503*, 365–370.

Corydon, T.J., Bross, P., Holst, H.U., Neve, S., Kristiansen, K., Gregersen, N., and Bolund, L. (1998). A human homologue of Escherichia coli ClpP caseinolytic protease: recombinant expression, intracellular processing and subcellular localization. Biochem. J. *331* (Pt 1), 309–316.

Craig, R., and Beavis, R.C. (2004). TANDEM: matching proteins with tandem mass spectra. Bioinform *20*, 1466–1467.

de Sagarra, M.R., Mayo, I., Marco, S., Rodriguez-Vilarino, S., Oliva, J., Carrascosa, J.L., and Casta ñ, J.G. (1999). Mitochondrial localization and oligomeric structure of HClpP, the human homologue of E. coli ClpP. J. Mol. Biol. *292*, 819–825.

DeLano, W.L. (2002). The PyMOL. Mol Graph Syst (DeLano Scientific).

Emsley, P., and Cowtan, K. (2004). Coot: model-building tools for molecular graphics. Acta Crystallogr. D Biol. Crystallogr. *60*, 2126–2132.

Emsley, P., Lohkamp, B., Scott, W.G., and Cowtan, K. (2010). Features and development of Coot. Acta Crystallogr. D Biol. Crystallogr. *66*, 486–501.

Eng, J.K., Jahan, T.A., and Hoopmann, M.R. (2013). Comet: an open-source MS/MS sequence database search tool. Proteomics *13*, 22–24.

Farge, T., Saland, E., de Toni, F., Aroua, N., Hosseini, M., Perry, R., Bosc, C., Sugita, M., Stuani, L., Fraisse, M., et al. (2017). Chemotherapy-resistant human acute myeloid leukemia cells are not enriched for leukemic stem cells but require oxidative metabolism. Cancer Discov. *7*, 716–735.

Frolova, O., Samudio, I., Benito, J.M., Jacamo, R., Kornblau, S.M., Markovic, A., Schober, W., Lu, H., Qiu, Y.H., Buglio, D., et al. (2012). Regulation of HIF-1alpha signaling and chemoresistance in acute lymphocytic leukemia under hypoxic conditions of the bone marrow microenvironment. Cancer Biol. Ther. *13*, 858–870.

Gersch, M., Famulla, K., Dahmen, M., Gobl, C., Malik, I., Richter, K., Korotkov, V.S., Sass, P., Rubsamen-Schaeff, H., Madl, T., et al. (2015). AAA chaperones and acyldepsipeptides activate the ClpP protease via conformational control. Nat. Commun. *6*, 6320.

Gersch, M., Stahl, M., Poreba, M., Dahmen, M., Dziedzic, A., Drag, M., and Sieber, S.A. (2016). Barrel-shaped ClpP proteases display attenuated cleavage specificities. ACS Chem. Biol. *11*, 389–399.

Greer, Y.E., Porat-Shliom, N., Nagashima, K., Stuelten, C., Crooks, D., Koparde, V.N., Gilbert, S.F., Islam, C., Ubaldini, A., Ji, Y., et al. (2018). ONC201 kills breast cancer cells *in vitro* by targeting mitochondria. Oncotarget *9*, 18454–18479.

Grochulski, P., Fodje, M.N., Gorin, J., Labiuk, S.L., and Berg, R. (2011). Beamline 08ID-1, the prime beamline of the Canadian macromolecular crystallography facility. J. Synchrotron Rad. *118*, 681–684.

Haynes, C.M., Petrova, K., Benedetti, C., Yang, Y., and Ron, D. (2007). ClpP mediates activation of a mitochondrial unfolded protein response in *C. elegans*. Dev. Cell *13*, 467–480.

Houtkooper, R.H., Mouchiroud, L., Ryu, D., Moullan, N., Katsyuba, E., Knott, G., Williams, R.W., and Auwerx, J. (2013). Mitonuclear protein imbalance as a conserved longevity mechanism. Nature *497*, 451–457.

Ishizawa, J., Kojima, K., Chachad, D., Ruvolo, P., Ruvolo, V., Jacamo, R.O., Borthakur, G., Mu, H., Zeng, Z., Tabe, Y., et al. (2016). ATF4 induction through an atypical integrated stress response to ONC201 triggers p53-independent apoptosis in hematological malignancies. Sci. Signal. *9*, ra17.

Jafari, R., Almqvist, H., Axelsson, H., Ignatushchenko, M., Lundback, T., Nordlund, P., and Martinez Molina, D. (2014). The cellular thermal shift assay for evaluating drug target interactions in cells. Nat. Protoc. *9*, 2100–2122.

Jin, S.M., and Youle, R.J. (2013). The accumulation of misfolded proteins in the mitochondrial matrix is sensed by PINK1 to induce PARK2/Parkin-mediated mitophagy of polarized mitochondria. Autophagy *9*, 1750–1757.

Kabsch, W. (2010). XDS. Acta Crystallogr. D Biol. Crystallogr. *66*, 125–132.

Kang, S.G., Dimitrova, M.N., Ortega, J., Ginsburg, A., and Maurizi, M.R. (2005). Human mitochondrial ClpP is a stable heptamer that assembles into a tetradecamer in the presence of ClpX. J. Biol. Chem. *280*, 35424–35432.

Kang, S.G., Maurizi, M.R., Thompson, M., Mueser, T., and Ahvazi, B. (2004). Crystallography and mutagenesis point to an essential role for the N-terminus of human mitochondrial ClpP. J. Struct. Biol. *148*, 338–352.

Kessner, D., Chambers, M., Burke, R., Agus, D., and Mallick, P. (2008). ProteoWizard: open source software for rapid proteomics tools development. Bioinformatics *24*, 2534–2536.

Kimber, M.S., Yu, A.Y., Borg, M., Leung, E., Chan, H.S., and Houry, W.A. (2010). Structural and theoretical studies indicate that the cylindrical protease ClpP samples extended and compact conformations. Structure *18*, 798–808.

Kline, C.L., Van den Heuvel, A.P., Allen, J.E., Prabhu, V.V., Dicker, D.T., and El-Deiry, W.S. (2016). ONC201 kills solid tumor cells by triggering an integrated stress response dependent on ATF4 activation by specific eIF2alpha kinases. Sci. Signal. *9*, ra18.

Kline, C.L.B., Ralff, M.D., Lulla, A.R., Wagner, J.M., Abbosh, P.H., Dicker, D.T., Allen, J.E., and El-Deiry, W.S. (2018). Role of dopamine receptors in the anticancer activity of ONC201. Neoplasia *20*, 80–91.

Konopleva, M., Contractor, R., Tsao, T., Samudio, I., Ruvolo, P.P., Kitada, S., Deng, X., Zhai, D., Shi, Y.X., Sneed, T., et al. (2006). Mechanisms of apoptosis sensitivity and resistance to the BH3 mimetic ABT-737 in acute myeloid leukemia. Cancer Cell *10*, 375–388.

Konopleva, M., Pollyea, D.A., Potluri, J., Chyla, B., Hogdal, L., Busman, T., McKeegan, E., Salem, A.H., Zhu, M., Ricker, J.L., et al. (2016). Efficacy and biological correlates of response in a phase ii study of venetoclax monotherapy in patients with acute myelogenous leukemia. Cancer Discov. *6*, 1106–1117.

Kotschy, A., Szlavik, Z., Murray, J., Davidson, J., Maragno, A.L., Le Toumelin-Braizat, G., Chanrion, M., Kelly, G.L., Gong, J.N., Moujalled, D.M., et al. (2016). The MCL1 inhibitor S63845 is tolerable and effective in diverse cancer models. Nature *538*, 477–482.

Kuntz, E.M., Baquero, P., Michie, A.M., Dunn, K., Tardito, S., Holyoake, T.L., Helgason, G.V., and Gottlieb, E. (2017). Targeting mitochondrial oxidative phosphorylation eradicates therapy-resistant chronic myeloid leukemia stem cells. Nat. Med. *23*, 1234–1240.

Lagadinou, E.D., Sach, A., Callahan, K., Rossi, R.M., Neering, S.J., Minhajuddin, M., Ashton, J.M., Pei, S., Grose, V., O'Dwyer, K.M., et al. (2013). BCL-2 inhibition targets oxidative phosphorylation and selectively eradicates quiescent human leukemia stem cells. Cell Stem Cell *12*, 329–341.

Lee, B.G., Park, E.Y., Lee, K.E., Jeon, H., Sung, K.H., Paulsen, H., Rubsamen-Schaeff, H., Brotz-Oesterhelt, H., and Song, H.K. (2010). Structures of ClpP in complex with acyldepsipeptide antibiotics reveal its activation mechanism. Nat. Struct. Mol. Biol. *17*, 471–478.

Lee, C.D., Sun, H.C., Hu, S.M., Chiu, C.F., Homhuan, A., Liang, S.M., Leng, C.H., and Wang, T.F. (2008). An improved SUMO fusion protein system for effective production of native proteins. Protein Sci. *17*, 1241–1248.

Leung, E., Datti, A., Cossette, M., Goodreid, J., McCaw, S.E., Mah, M., Nakhamchik, A., Ogata, K., El Bakkouri, M., Cheng, Y.Q., et al. (2011). Activators of cylindrical proteases as antimicrobials: identification and development of small molecule activators of ClpP protease. Chem. Biol. *18*, 1167–1178.

Lev, A., Lulla, A.R., Wagner, J., Ralff, M.D., Kiehl, J.B., Zhou, Y., Benes, C.H., Prabhu, V.V., Oster, W., Astsaturov, I., et al. (2017). Anti-pancreatic cancer activity of ONC212 involves the unfolded protein response (UPR) and is reduced by IGF1-R and GRP78/BIP. Oncotarget *8*, 81776–81793.

Marin-Valencia, I., Yang, C., Mashimo, T., Cho, S., Baek, H., Yang, X.L., Rajagopalan, K.N., Maddie, M., Vemireddy, V., Zhao, Z., et al. (2012). Analysis of tumor metabolism reveals mitochondrial glucose oxidation in genetically diverse human glioblastomas in the mouse brain *in vivo*. Cell Metabol. *15*, 827–837.

McCoy, A.J., Grosse-Kunstleve, R.W., Adams, P.D., Winn, M.D., Storoni, L.C., and Read, R.J. (2007). Phaser crystallographic software. J. Appl. Crystallogr. *40*, 658–674.

Moschoi, R., Imbert, V., Nebout, M., Chiche, J., Mary, D., Prebet, T., Saland, E., Castellano, R., Pouyet, L., Collette, Y., et al. (2016). Protective mitochondrial transfer from bone marrow stromal cells to acute myeloid leukemic cells during chemotherapy. Blood *128*, 253–264.

Müller, K., Faeh, C., and Diederich, F. (2007). Fluorine in pharmaceuticals: looking beyond intuition. Science *317*, 1881–1886.

Munch, C., and Harper, J.W. (2016). Mitochondrial unfolded protein response controls matrix pre-RNA processing and translation. Nature *534*, 710–713.

Ni, T., Ye, F., Liu, X., Zhang, J., Liu, H., Li, J., Zhang, Y., Sun, Y., Wang, M., Luo, C., et al. (2016). Characterization of gain-of-function mutant provides new insights into ClpP structure. ACS Chem. Biol. *11*, 1964–1972.

Pan, R., Hogdal, L.J., Benito, J.M., Bucci, D., Han, L., Borthakur, G., Cortes, J., DeAngelo, D.J., Debose, L., Mu, H., et al. (2014). Selective BCL-2 inhibition by ABT-199 causes on-target cell death in acute myeloid leukemia. Cancer Discov. *4*, 362–375.

Pan, R., Ruvolo, V., Mu, H., Leverson, J.D., Nichols, G., Reed, J.C., Konopleva, M., and Andreeff, M. (2017). Synthetic lethality of combined Bcl-2 inhibition and p53 activation in AML: mechanisms and superior antileukemic efficacy. Cancer Cell *32*, 748–760.e6.

Quiros, P.M., Mottis, A., and Auwerx, J. (2016). Mitonuclear communication in homeostasis and stress. Nat. Rev. Mol. Cell Biol. *17*, 213–226.

Roux, K.J., Kim, D.I., Raida, M., and Burke, B. (2012). A promiscuous biotin ligase fusion protein identifies proximal and interacting proteins in mammalian cells. J. Cell Biol. *196*, 801–810.

Samudio, I., Harmancey, R., Fiegl, M., Kantarjian, H., Konopleva, M., Korchin, B., Kaluarachchi, K., Bornmann, W., Duvvuri, S., Taegtmeyer, H., et al. (2010). Pharmacologic inhibition of fatty acid oxidation sensitizes human leukemia cells to apoptosis induction. J. Clin. Invest. *120*, 142–156.

Seiferling, D., Szczepanowska, K., Becker, C., Senft, K., Hermans, S., Maiti, P., Konig, T., Kukat, A., and Trifunovic, A. (2016). Loss of CLPP alleviates mitochondrial cardiomyopathy without affecting the mammalian UPRmt. EMBO Rep. *17*, 953–964.

Skrtic, M., Sriskanthadevan, S., Jhas, B., Gebbia, M., Wang, X., Wang, Z., Hurren, R., Jitkova, Y., Gronda, M., Maclean, N., et al. (2011). Inhibition of mitochondrial translation as a therapeutic strategy for human acute myeloid leukemia. Cancer Cell *20*, 674–688.

Sprangers, R., Gribun, A., Hwang, P.M., Houry, W.A., and Kay, L.E. (2005). Quantitative NMR spectroscopy of supramolecular complexes: dynamic side pores in ClpP are important for product release. Proc. Natl. Acad. Sci. U S A *102*, 16678–16683.

Sriskanthadevan, S., Jeyaraju, D.V., Chung, T.E., Prabha, S., Xu, W., Skrtic, M., Jhas, B., Hurren, R., Gronda, M., Wang, X., et al. (2015). AML cells have low spare reserve capacity in their respiratory chain that renders them susceptible to oxidative metabolic stress. Blood *125*, 2120–2130.

Stein, M.N., Bertino, J.R., Kaufman, H.L., Mayer, T., Moss, R., Silk, A., Chan, N., Malhotra, J., Rodriguez, L., Aisner, J., et al. (2017). First-in-human clinical trial of Oral ONC201 in patients with refractory solid tumors. Clin. Cancer Res. *23*, 4163–4169.

Tu, Y.S., He, J., Liu, H., Lee, H.C., Wang, H., Ishizawa, J., Allen, J.E., Andreeff, M., Orlowski, R.Z., Davis, R.E., et al. (2017). The imipridone ONC201 induces apoptosis and overcomes chemotherapy resistance by up-regulation of bim in multiple myeloma. Neoplasia *19*, 772–780.

Viale, A., Pettazzoni, P., Lyssiotis, C.A., Ying, H., Sanchez, N., Marchesini, M., Carugo, A., Green, T., Seth, S., Giuliani, V., et al. (2014). Oncogene ablation-resistant pancreatic cancer cells depend on mitochondrial function. Nature *514*, 628–632.

Wagner, J., Kline, C.L., Ralff, M.D., Lev, A., Lulla, A., Zhou, L., Olson, G.L., Nallaganchu, B.R., Benes, C.H., Allen, J.E., et al. (2017). Preclinical evaluation of the imipridone family, analogs of clinical stage anti-cancer small molecule ONC201, reveals potent anti-cancer effects of ONC212. Cell Cycle *16*, 1790–1799.

Wang, K., Li, M., and Hakonarson, H. (2010). ANNOVAR: functional annotation of genetic variants from high-throughput sequencing data. Nucleic Acids Res. *38*, e164.

Warner, J.K., Wang, J.C., Takenaka, K., Doulatov, S., McKenzie, J.L., Harrington, L., and Dick, J.E. (2005). Direct evidence for cooperating genetic events in the leukemic transformation of normal human hematopoietic cells. Leukemia *19*, 1794–1805.

Winn, M.D., Ballard, C.C., Cowtan, K.D., Dodson, E.J., Emsley, P., Evans, P.R., Keegan, R.M., Krissinel, E.B., Leslie, A.G., McCoy, A., et al. (2011). Overview of the CCP4 suite and current developments. Acta Crystallogr. D Biol. Crystallogr. *67*, 235–242.

Wong, K.S., Mabanglo, M.F., Seraphim, T.V., Mollical, A., Mao, Y., Rizzolo, K., Leung, E., Moutaoufik, M.T., Hoell, L., Phanse, S., et al. (2018). Acyldepsipeptide analogs dysregulate human mitochondrial ClpP protease activity and cause apoptotic cell death. Cell Chem. Biol. *25*, 1017–1030.

Zhao, Q., Wang, J., Levichkin, I.V., Stasinopoulos, S., Ryan, M.T., and Hoogenraad, N.J. (2002). A mitochondrial specific stress response in mammalian cells. EMBO J. *21*, 4411–4419.

STAR★METHODS

KEY RESOURCES TABLE

REAGENT or RESOURCE	SOURCE	IDENTIFIER
Antibodies		
Antibody Cocktail	Abcam, Cambridge, UK	ab110413; RRID: AB_2629281
Anti-SDHA	Abcam, Cambridge, UK	ab14715; RRID: AB_301433
Anti-ATF4	Cell Signaling, Danvers, MA	11815 D4B8; RRID: AB_2058593
Anti-eIF2α	Cell Signaling, Danvers, MA	9722; RRID: AB_2716733
Anti-phospho-eIF2a (S51)	Abcam, Cambridge, UK	ab32157, E90; RRID: AB_732117
Anti-ClpP	Abcam, Cambridge, UK	ab124822; RRID: AB_10975619
Anti-β-actin	Millipore-Sigma, Darmstadt, Germany	A5316, AC-74; RRID: AB_476743
Anti-GAPDH	Cell Signaling, Danvers, MA	2118, 14C10; RRID: AB_2107303
Total OXPHOS Rodent WB Antibody Cocktail	Abcam, Cambridge, UK	ab110413; RRID: AB_2629281
Anti-SDHB	Abcam, Cambridge, UK	ab14714; RRID: AB_301432
Anti-NDUFA12	Abcam, Cambridge, UK	ab192617; RRID: AB_1079551
Anti-NDUFB8	Abcam, Cambridge, UK	Ab152558, ab110242; RRID: AB_10859122
Anti-UQCRC2 antibody	Abcam, Cambridge, UK	Ab14745; RRID: AB_2213640
Anti-MTC01	Abcam, Cambridge, UK	Ab14705; RRID: AB_2084810
Anti-CS	Abcam, Cambridge, UK	ab129095; RRID: AB_11143209
Anti-ClpP	Millipore-Sigma, Darmstadt, Germany	HPA010649, ab 126102; RRID: AB_11130135
Chemicals, Peptides, and Recombinant Proteins		
ONC201	Oncoceutics, Philadelphia, PA	NA
	MedChemExpress, Monmouth Junction, NJ	HY-15615A
ONC212	Oncoceutics, Philadelphia, PA	NA
ONC201 isomer (inactive analog)	MedChemExpress, Monmouth Junction, NJ	HY-15615
DMSO	Millipore-Sigma, Darmstadt, Germany	D2650
FCCP (Seahorse XFp Cell Energy Phenotype Test Kit)	Agilent Technologies, INC. Santa Clara, CA	103275-100
Penicillin-Streptomycin	ThermoFisher, Waltham, MA	15140122
cOmplete™, Mini Protease Inhibitor Cocktail	Millipore-Sigma, Darmstadt, Germany	11836153001
Proteinase Inhibitors	ThermoFisher, Waltham, MA	78425
PBS	Corning, Corning, NY	21-040-CV
Antimycin A	Millipore-Sigma, Darmstadt, Germany	A8674
Hygromycin B	Bioshop Canada Inc., Burlington, ON	HYG005
Tryptone	BioShop Canada Inc, Burlington, Canada	TRP402
Yeast Extract	BioShop Canada Inc, Burlington, Canada	YEX555
Luria-Bertrani Broth	Wisent Bioproducts, ST-BRUNO, Quebec Canada	809-060-CL
Kanamycin	BioShop Canada Inc, Burlington, Canada	KAN201
Isopropyl-1-thio-B-D-galactopyranoside (IPTG)	BioShop Canada Inc, Burlington, Canada	IPT002
DL-Dithiothreitol (DTT)	BioShop Canada Inc, Burlington, Canada	DTT002
HisPur™ Ni-NTA Res	ThermoFisher, Waltham, MA	88222
Triton X-100	BioShop Canada Inc, Burlington, Canada	TRX777
Oligomycin (Seahorse XFp Cell Energy Phenotype Test Kit)	AGILENT TECHNOLOGIES, INC. Santa Clara, CA	103275-100
β-Mercaptoethanol	ThermoFisher, Waltham, MA	21985-023
Bromophenol Blue	Millipore-Sigma, Darmstadt, Germany	114391

(*Continued on next page*)

Continued

REAGENT or RESOURCE	SOURCE	IDENTIFIER
Human Flt3-Ligand, premium grade	Il-Miltenyi Biotec, San Diego, CA	130-096-479
Human IL-7, premium grade	Miltenyi Biotec, San Diego, CA	130-095-363
Recombinant Human IL-3 Protein	R&D Systems, Minneapolis, MN	203-IL
Human IL-6, premium grade	Miltenyi Biotec, San Diego, CA	130-093-932
G-CSF (Neupogen)	Amgen Inc.	Thousand Oaks, CA
Human GM-CSF, premium grade	Miltenyi Biotec, San Diego, CA	130-093-866
Tetracycline	Millipore-Sigma, Darmstadt, Germany	D9891
Annexin V APC	ThermoFisher, Waltham, MA	A35110
Annexin V FITC	Beckman Colter, Brea, CA	IM3546
Propidium Iodide (PI)	Millipore-Sigma, Darmstadt, Germany	P4170
FBS	Millipore-Sigma, Darmstadt, Germany	F2442
RPMI 1640	Corning, Corning, NY	10-040-CV
IMDM	ThermoFisher, Waltham, MA	I6529
Luciferin	Gold biotechnology, St. Louis, MO	LUCK
Untagged human mitochondrial ClpP (ClpP)	(Wong et al., 2018)	N/A (produced in house)
Yeast SUMO protease	(Lee et al., 2008)	N/A (produced in house)
α-Casein	Millipore-Sigma, Darmstadt, Germany	C6780
Glycerol	Millipore-Sigma, Darmstadt, Germany	G5516
Glycerol Imidazole	BioShop Canada Inc, Burlington, Canada	Cat#GLY002
Glycerol Imidazole NaCl	BioShop Canada Inc, Burlington, Canada	IMD508
Glycerol Imidazole NaCl Tris Hydrochloride	BioShop Canada Inc, Burlington, Canada	SOD001
Glycerol Imidazole NaCl Tris Hydrochloride HCl	BioShop Canada Inc, Burlington, Canada	TRS004
Glycerol	BioShop Canada Inc, Burlington, Canada	HCL333
Imidazole NaCl Tris Hydrochloride HCl BisTris	BioShop Canada Inc, Burlington, Canada	BST666
KCl	BioShop Canada Inc, Burlington, Canada	POC308
Sodium Acetate	BioShop Canada Inc, Burlington, Canada	SAA555
MgCl2	Millipore-Sigma, Darmstadt, Germany	M1028
DMSO	Millipore-Sigma, Darmstadt, Germany	CAS 67-68-5
Creatine phosphate	Millipore-Sigma, Darmstadt, Germany	10621714001
Creatine kinase	Lee Biosolutions, Maryland Heights, USA	190-10
Tween 20	Millipore-Sigma, Darmstadt, Germany	P1379
PEG4000	Millipore-Sigma, Darmstadt, Germany	CAS 25322-68-3
Recombinant Human SCF Protein (TEX)	R&D Systems, Minneapolis, MN	255-sc/cf
L-Glutamine 200mM (TEX)	ThermoFisher Scientific	25030081
L-Glutamine	ThermoFisher, Waltham, MA	21051024
MitoSox Red	ThermoFisher, Waltham, MA	M36008
Ac-Trp-Leu-Ala-AMC (Ac-WLA-AMC)	Boston Biochem	S-330 lot 10066817
Ac-Phe-hArg-Leu-ACC	Life Technologies Inc.	PEP97MODMM

(*Continued on next page*)

Continued

REAGENT or RESOURCE	SOURCE	IDENTIFIER
FITC-casein	Millipore-Sigma, Darmstadt, Germany	C0528
Clptide	Biomatik Corp., Cambridge, Canada	511266
Mca-Pro-Leu-Gly-Pro-D-Lys(Dnp)-OH	Bachem Americas, Inc, Torrance, USA	4027687
Seahorse Assay Medium	AGILENT TECHNOLOGIES, INC. Santa Clara, CA	102365-100
Sodium uccinate	Millipore-Sigma, Darmstadt, Germany	14160-100G
HEPES	Bioshop	HEP001.1
bovine serum albumin	Millipore-Sigma, Darmstadt, Germany	A3803-10G
Rotenone	Millipore-Sigma, Darmstadt, Germany	R8875-1G
KCN	Millipore-Sigma, Darmstadt, Germany	60718-25G
2,6-dichloroindophenol	Millipore-Sigma, Darmstadt, Germany	D1878-5G
Decylubiquinone	Millipore-Sigma, Darmstadt, Germany	D7911-10mg
ferricytochrome c	Millipore-Sigma, Darmstadt, Germany	C7752
dodecyl-D-maltoside	Millipore-Sigma, Darmstadt, Germany	D4641
L-ascorbic acid	Millipore-Sigma, Darmstadt, Germany	A5960-25G
Sodium Malonate	Millipore-Sigma, Darmstadt, Germany	63409-100G
Primers		
CLPP cDNA fwd	Integrated DNA Technologies, Coralville, USA	5'- ACTGAATTCGCCACCATGTGG CCCGGAATATTGGT-3'
CLPP cDNA rev	Integrated DNA Technologies, Coralville, USA	5'- ATCGGATCCTCTCAGGTGCTA GCTGGGAC-3'
InFusion *CLPP* fwd	Integrated DNA Technologies, Coralville, USA	5'-TAGAGCTAGCGAATTGCCACCA TGTGGCCCGGAATATT-3'
InFusion *CLPP* rev	Integrated DNA Technologies, Coralville, USA	5'-CGGCGGCCGCGGATCTCAGGTG CTAGCTGGGACAG-3'
CLPP mut D190A fwd	Integrated DNA Technologies, Coralville, USA	5'-GGGCCAAGCCACAGCCATTGCCA TCCAGGCAG-3'
CLPP mut D190A rev	Integrated DNA Technologies, Coralville, USA	5'-CTGCCTGGATGGCAATGGCTGTG GCTTGGCCC-3'
CLPP 890 rev seq	Integrated DNA Technologies, Coralville, USA	5'-GGCTCATCCTCACCGTCCTG-3'
CLPP 540 rev seq	Integrated DNA Technologies, Coralville, USA	5'-GATGTACTGCATCGTGTCGT-3'
Critical Commercial Assays		
Alamar-Blue Assay	ThermoFisher Sci	DAL1025
DNA Fingerprinting (Promega Powerplex 16 HS kit)	Promega, Madison, WI	DC2101
Complex I Enzyme Activity Microplate Assay Kit	Abcam, Cambridge, UK	ab109721
Deposited Data		
X-ray structure: human mitochondrial ClpP in complex with ONC201	This paper	PDB: 6DL7
X-ray structure: ClpP in complex with ADEP-28	(Wong et al., 2018)	PDB: 6BBA
Mass spectrometry analysis (related to Figure 5A)	MassIVE archive (massive.ucsd.edu)	MSV000082381
RNA-seq dataset of Z138 cells	Sequence Read Archive (SRA)	SUB4176298
Experimental Models: Cell Lines		
Z138 Cells	ATCC, Manassas, VA	NA
OCI-AML2	Lab stock	NA
OCI-AML3	DSMZ, Braunschweig, Germany	NA
TEX Cells	Ontario Cancer Institute, Toronto, Canada	Gift
T-REx HEK293	CECAD Research Center, Cologne Germany	Gift

(*Continued on next page*)

Continued

REAGENT or RESOURCE	SOURCE	IDENTIFIER
HEK293T Cells	ATCC, Manassas, VA	NA
HCT116	Lab stock	NA
OC316	Lab stock	NA
SUM159	Lab stock	NA
Experimental Models: Organisms/Strains		
NSG Mice	The Jackson Laboratory, Bar Harbor, ME	NA
E. coli BL(DE3) *ΔclpP::cat* (SG1146)	(Kimber et al., 2010)	NA
Human Primary Cells	This paper	NA
Recombinant DNA		
pETSUMO	(Lee et al., 2008)	N/A
pETSUMO2-CLPP(-MTS)	(Wong et al., 2018)	N/A
Software and Algorithms		
GraphPad Prism 7	GraphPad , Inc. La Jolla, CA	NA
CCP4 Suite	(Winn et al., 2011)	http://www.ccp4.ac.uk/
XDS	(Kabsch, 2010)	
PHENIX Software Package	(Adams et al., 2010)	https://www.phenix-online.org/
Phaser	(McCoy et al., 2007)	https://www.phenix-online.org/
Coot	(Emlsey et al., 2010)	https://www2.mrc-lmb.cam.ac.uk/personal/pemsley/coot/
PyMol	(DeLano, 2002)	https://pymol.org/2/
Rnaseqmut		https://github.com/davidliwei/rnaseqmut
Origin7 MicroCal Analysis Software	Malvern, Malvern, UK	NA
ANNOVAR	(Wang et al., 2010)	
Proteowizard	ProteoWizard release: 3.0.10800 (2017-4-27)	http://proteowizard.sourceforge.net/
X!Tandem	X! TANDEM Jackhammer TPP (2013.06.15.1 - LabKey, Insilicos, ISB)	https://www.thegpm.org/tandem/
Comet	Comet version "2014.02 rev. 2"	http://comet-ms.sourceforge.net/
SAINT	SAINT Version:2.5.0, Express Version:exp3.6.1	http://prohitsms.com
Cytoscape	Cytoscape 3.6.0	http://www.cytoscape.org

CONTACT FOR REAGENT AND RESOURCE SHARING

Further information and requests for reagents may be directed to, and will be fulfilled by the lead contact Michael Andreeff (mandreef@mdanderson.org).

EXPERIMENTAL MODEL AND SUBJECT DETAILS

Mice

For all the animal studies in the present study, the study protocols were approved by the Institutional Animal Care and Use Committee (IACUC) at the Princess Margaret Cancer Center and MD Anderson Cancer Center.

Two million Z138 cells transfected with the WT or D190A mutant *CLPP*-over-expressing vector and labeled with luciferase were injected to individual NSG mice (n = 7 per treatment group, all female). After confirming engraftment measured by *in vivo* bioluminescence imaging on d 9 post-transplantation, ONC212 (50mg/kg/d) or vehicle (water) is administered by oral gavage every other d until the mice got moribund. Tumor burden measured by luminescence was followed weekly until d 31. Independently, two million Z138 cells transfected with tetracycline-inducible Y118A mutant ClpP were labeled with luciferase and injected to individual NSG mice (n = 10 per treatment group, all male). After confirming engraftment measured by *in vivo* bioluminescence imaging on day 5 post-transplantation, the mice were treated with or without tetracycline (2 mg/mL) in drinking water until moribund. One million OCI-AML2 cells were injected to individual SCID mice (n = 10 per treatment group, all male). Five days after injection, mice were treated with ONC201 twice daily with ONC201 by oral gavage (100 mg/kg) for 13 days. Engraftment experiments using patient-derived xenograft AML cells were performed as previously reported (Ishizawa et al., 2016). Primary AML cells were transplanted

into female 6-week-old NSG mice, and leukemia cells were harvested from secondarily transplanted mice. Leukemic cells were treated with or without 250 nM of ONC212 for 36 hr, then 0.7 million trypan blue–negative cells were injected via tail vein into each of 7 NSG mice per treatment group. The mice in each group were monitored for survival.

Human Subjects and Primary Samples

The data derived from the second patient enrolled in the clinical trial at MD Anderson Cancer Center (NCT02392572) was presented in Figure S8. The study was conducted in accordance with the Declaration of Helsinki and was approved by an Institutional Review Board at MD Anderson Cancer Center. Informed consent was obtained from all patients.

Bulk AML cells from AML patients and peripheral blood stem cells from healthy G-CSF-treated stem cell donors were isolated by Ficoll density centrifugation and apheresis, respectively. Isolated cells were maintained in IMDM supplemented with 10% FBS, or Myelocult H5100 (Stemcell Technologies, Vancouver, BC) , supplemented with 100 ng/mL SCF, 10 ng/mL FLT3-L, 20 ng/mL IL-7, 10 ng/mL IL-3, 20 ng/mL IL-6, 20 ng/mL G-CSF, 20 ng/mL GM-CSF. Cells were supplemented with 100 μg/ml penicillin, and 100 U/ml streptomycin, at 37°C and 5% CO2 in humidified atmosphere. The University Health Network (Toronto, ON) and MD Anderson Cancer Center (Houston, Texas) institutional review boards approved the collection and use of human tissue for this study. All samples were obtained from consenting patients.

Bacterial Cell Culture

For the expression and purification of human mitochondrial ClpP protein, *E. coli* SG1146 carrying pETSUMO2-CLPP(-MTS) were grown aerobically in Luria-Bertrani Broth (LB; 10 g/L tryptone, 5 g/L yeast extract, 10 g/L NaCl) supplemented with 50 μg/mL kanamycin at 37°C with shaking at 180 rpm.

METHOD DETAILS

Protein Purification and Crystallization

Human ClpP was expressed and purified as described previously (Kang et al., 2004; Kimber et al., 2010; Wong et al., 2018). Wildtype and mutant (Y118A and D190A) human ClpP (without mitochondrial targeting sequences) were cloned into pETSUMO2 expression vectors and expressed in *E. coli* SG1146 (Kimber et al., 2010). To induce protein expression, bacteria, after reaching $OD_{600} \sim 0.6$, were treated with 1mM isopropyl-1-thio-B-D-galactopyranoside for 4 h at 37°C, harvested by centrifugation, and disrupted in lysis buffer (25 mM Tris-HCl (pH 7.5), 0.5 M NaCl, 10 mM imidazole, 10% glycerol) by Emulsiflex C5 (4 passes; Avestin, Ottawa, Canada). Following cell lysis, the insoluble material was removed by centrifugation (26,892 x g (Sorvall rotor SS-34) for 30 min) and the supernatant was passed through a 5 mL Ni-sepharose high-performance (GE) column pre-equilibrated with lysis buffer. The protein was eluted with 400 mM imidazole, diluted with 25 mL of dialysis buffer (25 mM Tris-HCl (pH 7.5), 0.1 M NaCl, 10% glycerol), mixed with SUMO protease (1:100 ; Lee et al., 2008), and dialyzed overnight at 4°C with light stirring into 4 L of dialysis buffer using SnakeSkin 10K dialysis membrane (ThermoScientific, Waltham, MA). The dialyzed material was then passed through a second 5 mL Ni-column (ThermoScientific, Waltham, MA) and the flow-through solution containing untagged ClpP was collected. All fractions were analyzed by SDS-PAGE.

For crystallography, protein was concentrated using an Amicon Ultra-15 30K concentrator (Sigma-Aldrich) and further purified using an anion exchange 5 mL QSepharoseHP HiTrap (Amersham Biosciences, Little Chalfont, UK) column with a linear gradient from 100 mM to 1 M NaCl in 20 mM Tris-HCl (pH 7.5). Protein eluted at about 200 mM NaCl concentration.

It was then pre-concentrated using Amicon Ultra-15 30K concentrators and dialyzed at 4°C overnight into 25 mM Bis-Tris, pH 6.5, containing 3 mM DTT. ClpP was then further concentrated to 12 mg/mL. ONC201, solubilized in 100% DMSO, was added to the concentrated protein to bring the final concentration of the compound to 2.5 mM with a DMSO concentration of 5%.

The ClpP-ONC201 complex was crystallized at 4°C by the hanging drop vapor diffusion method. 2 μL of protein-drug solution were mixed with 2 μL of reservoir solution. Wells containing reservoir solutions of 500 μL of 5% (w/v) PEG 4,000, 100 mM KCl, and 100 mM NaAc (pH 5.2) produced crystals of 100-200 μm in all three dimensions. Crystals appeared in 2-3 weeks and were harvested into reservoir solutions containing 2.5 mM ONC201, 5% DMSO, and 20% glycerol for cryo-protection. Crystals in standard cryo-loops were flash-frozen in liquid nitrogen.

Collection and Processing of Diffraction Data

Diffraction data were obtained at beamline 08ID-1 of the Canadian Light Source (Saskatoon, Canada; Grochulski et al., 2011) at 100 K and recorded with the help of a Pilatus3 S 6M detector (Dectris, Switzerland). The wavelength was 0.9795 Å and 2500 images were collected with a 0.1° oscillation range and 0.2 s exposures. Crystal to detector distance was 392.6 mm. Data were indexed, integrated, and scaled using the XDS (Kabsch, 2010) and CCP4 (Winn et al., 2011) software packages. The protein complex crystallized in space group C2 with one ClpP heptamer ring in the asymmetric unit (ASU), as had previously been seen for the closed conformation of human mitochondrial ClpP (PDB-ID:1TG6)(Kang et al., 2004).

Structure Solution and Refinement

The crystal structure of the ClpP-ONC201 complex was solved by molecular replacement using the PHENIX software package (Adams et al., 2010; McCoy et al., 2007). The same software was applied for refinement and validation and the package COOT

(Emsley and Cowtan, 2004; Emsley et al., 2010) for model building. Starting phases for structure determination were calculated using the activated ClpP heptamer structure with waters removed as the search model (PDB: 6BBA; Wong et al., 2018). Riding hydrogens were used during the last several rounds of refinement (Afonine and Adams, 2012) to optimize the geometry but were not included in the final deposited coordinate file. See Table S4 for data reduction and refinement statistics. PyMol v1.3 software was used to generate structure figures (DeLano, 2002). Coordinates and structure factors of the ClpP-ONC201 complex structure were deposited into the RCSB - Protein Data Bank with Accession No. 6DL7.

Chemical Screen

Assay buffer consisted of 25 mM HEPES pH 7.4, 5 mM $MgCl_2$, 5 mM KCl, 0.03% Tween 20, 10% glycerol, 16 mM creatine phosphate, 13 U/ml creatine kinase, and 3 mM ATP. 1.0 μM human ClpP (Cole et al., 2015) was dissolved in the assay buffer using Biomek FX robotic liquid handler (Beckman Coulter Life Sciences, Indianapolis, IN) and mixed with 0.625 mM and 1.25 mM-concentrations of each compounds in 384- well plates using Beckman Multimek 96/384 liquid handling system (Beckman Coulter Life Sciences, Indianapolis, IN) at 0.2 μL per well (final concentrations 4.15 and 8.3 μM, respectively) and incubated at 37C for 10 min. Fluorescent tagged- substrates, FITC-casein (4.0 μM) was then added to each well and fluorescence was measured at 485/535 nm every 5 min for 70 min at 37°C using PHERAstar microplate reader (BMG LABTECH, Ortenberg, Germany)

ClpP Enzymatic Assays

Assay buffer consisted of 25 mM HEPES pH 7.5, 5 mM $MgCl_2$, 5 mM KCl, 0.03% Tween 20, 10% glycerol, 16 mM creatine phosphate,13 U/ml creatine kinase, and 3 mM ATP for FITC-Casein assay, 100mM KCl, 5 % glycerol, 10mM MgCl2, 20mM Triton X-100, and 50mM TRIS pH 8 for AC-WLA-AMC assay, 50 mM Tris, pH 8 , 300 mM KCl, and 15% glycerol for Ac-Phe-hArg-Leu-ACC assay, 50 mM Hepes, pH 7.5 with 5 mM ATP, 0.03% Tween 20, 15 mM MgCl2 , 100 mM KCl and 5% Glycerol for FAPHMALVPV (Clptide) assay, and 25 mM Tris, pH 7.5 with 150 mM NaCl for MCA-Pro-Leu-Gly-Pro-D-Lys assay (Gersch et al., 2016).

For fluorescence assays, 0.7 μM (for FITC-casein, AC-WLA-AMC, and Ac-Phe-hArg-Leu-ACC assays) or 7.0 μM (for FAPHMALVPV and MCA-Pro-Leu-Gly-Pro-D-Lys assays) human ClpP was dissolved in the assay buffer, incubated at 37°C for 10 min, and mixed with increasing concentrations of ONC201, ONC201 isomer, and ONC212 (0-100 μM) in 96 well plates at 50 μL per well in triplicate. Fluorescent tagged- substrates, FITC-casein (4.5 μM) or AC-WLA-AMC (15mM) (Wong et al., 2018), Ac-Phe-hArg-Leu-ACC (100 μM), FAPHMALVPV (50 μM) and MCA-Pro-Leu-Gly-Pro-D-Lys (25 μM) were then added to each well and fluorescence was measured at 485/535 nm for FITC casein assay, at 360/440 nm for AC-WLA-AMC assay, at 380/440 nm for Ac-Phe-hArg-Leu-ACC assay, at 320/420 nm for FAPHMALVPV (Clptide) assay, and at 320/405 nm for MCA-Pro-Leu-Gly-Pro-D-Lys assay every 30 s for 90 min at 37°C using a monochromator microplate reader (Clariostar BMG LABTECH, Ortenberg, Germany). Hill coefficient was determined using Origin7, Pharmacology – Dose-response curve with log (compound concentration) as the independent variable.

For gel-based assays, 1.5 μM ClpP, alone and in combination with 4.5 μM ClpX, was mixed with 22 μM unlabeled bovine α-casein and treated with 0.2 and 6.3 μM concentrations of ONC201 and ONC212 in FITC-casein assay buffer (See above). The mixture was incubated at 37°C for 3 h, loaded on 12% SDS-PAGE, run at 120V, and stained with Coomassie Blue.

Isothermal Titration Calorimetry (ITC)

ITC binding measurements were performed using the MicroCal VP-ITC system (Malvern, Malvern, UK). Aliquots of purified wild type and D190A ClpP were dialyzed separately overnight at 4°C with light stirring into 20 mM TrisHCl, 5% DMSO, pH 7.65 (pH at room temperature) using SnakeSkin 10K dialysis membrane (ThermoFisher, Waltham, MA). The VP-ITC cell was filled with 20 μM ClpP (WT or D190A; ClpP monomer concentration) and 100 μM ONC201 was used in the syringe. The following setup was used: Injection volume: 281.55 μL, Cell volume: 1.4551 mL, Spacing time between injections: 240 s, 27 injections: 10 μL over 20 s each; 1st 2 μL over 4 s, filter period – 2 s, steering speed – 307, temperature – 25°C, reference power – 15 μCal/s. In the reversed experiment 500 μM WT ClpP in the syringe was titrated into 50 μM ONC201 solution; same instrument setup was used for these experiments. Control experiments were carried out to account for dilution effects upon ligand into protein and protein into ligand titration. Data were analyzed with Origin7 MicroCal Analysis software.

Gel Filtration

0.4 mg of WT or D190A ClpP in 400 μL (with or without ONC201 in 1:1 molar ratio – ClpP monomer to ONC201 ratio; in running buffer) was loaded onto the analytical size exclusion column Superdex 200 10/300 GL (Amersham Biosciences, Little Chalfont, UK) and run at RT at 0.5 mL/min in running buffer (20 mM TrisHCl, 100 mM NaCl, pH7.5).

Cell Culture

OCI-AML2 cells were grown in Iscove's Modified Dulbecco's Medium (IMDM) with 10% FBS. OCI-AML3, HCT116, OC316 and SUM159 cells were cultured in RPMI medium with 10% FBS. TEX cells(Warner et al., 2005) were provided by Dr. John Dick (Ontario Cancer Institute, Toronto, Canada) and grown in IMDM supplemented with 15% FCS, 2 mM L-glutamine, 20 ng/ml stem cell factor (SCF), and 2 ng/ml IL-3 (R&D Systems, Minneapolis, MN). Z138 cells were cultured in RPMI with 20% FBS. T-REx HEK293 cells were grown in DMEM with 10% FBS.

ClpP -/- and ClpP / T-REx HEK293 cells were a gift from Dr. Aleksandra Trifunovic's lab (CECAD Research Center, University of Cologne, Germany). All the other cell lines were purchased from Leibniz-Institut Deutsche Sammlung von Mikroorganismen und Zellkulturen (DSMZ, Braunschweig, Germany) or the American Type Culture Collection (ATCC, Manassas, VA).100units/mL penicillin and 100ug/mL streptomycin was added to the media for all cells lines. All cells were cultured at 37°C and 5% CO2. The authenticity of the cell lines was confirmed by DNA fingerprinting with the short tandem repeat method, using a PowerPlex 16 HS System (Promega, Madison, WI) within 6 m before the experiments.

Cell Viability Assays

For Alamar-Blue assays, cells (1 x 10^4 / well) were plated in 96-well plates (final volume of 100 μL/well), and treated with increasing concentrations of ONC201 and ONC212 (0 to 100μM). After a 72-hr period of incubation at 37°C, 10μL of Alamar Blue was added to the culture medium and the mixture was incubated for an additional 2 h at 37°C. Cytotoxicity was measured using spectrophotometry of fluorescence at excitation 560 nm and emission 590 nm (SpectraMax M3, Molecular Devices, San Jose, CA). For apoptosis analysis, annexin V and PI binding assays were performed to assess apoptosis as described previously (Ishizawa et al., 2016). Cells (1.5 x 10^5 / well for AML cells in 24-well plates and 0.8 x 10^5 for HCT116 cells in 12-well plates) were plated and treated with ONC201 and ONC212. Annexin V and PI were stained after 72 hr incubation. Annexin V- and PI-negative cells were counted as live cells.

Cellular Thermal Shift Assay (CETSA)

CETSA was conducted as previously described (Jafari et al., 2014). OCI-AML2 cells were treated with increasing concentrations of ONC201 or ONC212 for 30 min at 37°C. Cells were then washed and re-suspended in PBS containing proteinase inhibitors and heated to 67°C for 3 min using a thermal cycler (SimpliAmp, Applied Biosystems). This temperature was experimentally derived by heating cells pretreated with the drug for 1 h at different temperatures to determine the optimal thermal shift of the protein. Following this step, cells were lysed by 4 freeze-thaw cycles with vortexing and pure cell lysates were collected after centrifugation at 16,000 x *g* for 30 min at 4°C.

In wash-off experiments, ONC201 (10 μM) treated cells were washed in PBS, pelleted and re-suspended in fresh media and incubated for increasing time intervals starting from 15-75 min at 37°C. After this, cells were again washed and re-suspended in PBS containing proteinase inhibitors, heated to 67°C for 3 min, and cell lysates were collected as described above.

RNA-Sequencing

Barcoded, Illumina compatible, strand-specific total RNA libraries were prepared using the TruSeq Stranded Total RNA Sample Preparation Kit (Illumina, San Diego, CA). Briefly 1μg of DNase I treated total RNA was depleted of cytoplasmic and mitochondrial ribosomal RNA (rRNA) using Ribo-Zero Gold (Illumina). After purification, the RNA was fragmented using divalent cations and double stranded cDNA was synthesized using random primers. The ends of the resulting double stranded cDNA fragments were repaired, 5′-phosphorylated, 3'-A tailed and Illumina-specific indexed adapters were ligated. The products were purified and enriched by 11 cycles of PCR to create the final cDNA library. The libraries were quantified using the Qubit dsDNA HS Assay Kit (ThermoFisher) and assessed for size distribution using the Fragment Analyzer (Advanced Analytical, Ankeny, IA), then multiplexed 4 libraries per pool. Library pools were quantified by qPCR and sequenced, one pool per lane, on the Illumina HiSeq4000 sequencer using the 75 bp paired end format. For each sample, TopHat was used to align reads from FASTQ files to the reference genome (hg19) and generate BAM files. These were then used as input to rnaseqmut, which identifies genomic nucleotide positions at which a minimum number and proportion of reads have a variant sequence, i.e., indels or single-nucleotide variants (SNVs). There was no filtering to exclude known single-nucleotide polymorphisms (SNPs). For each SNV identified in either or both of the parental or ONC201-resistant samples of Z138 cells, rnaseqmut provided the number of reads (forward and backward) with a WT nucleotide in that position, and the number of reads with the SNV in that position, for each sample. If the total number of reads at that position exceeded a minimum number of total reads (20), Fisher's exact test was used to compare the difference in the mutant allele frequency (MAF) in parental vs. resistant cells. SNVs meeting the criteria for minimum read number and Fisher test-significant MAF difference in either direction (i.e., higher in either the drug-naïve or resistant cells) were further characterized by ANNOVAR (Wang et al., 2010) as to whether they were intergenic, intronic, in the 5' or 3' UTR, or within exons, and if the latter, whether they were synonymous (silent), nonsynonymous (NSV), or involved the gain or loss of a stop codon.

Site Directed Mutagenesis

All point mutations were induced using Phusion High Fidelity DNA polymerase or QuikChange II site directed mutagenesis kit (Agilent Technologies, Santa Clara, CA) using the manufacture's protocol (New England Biolabs, Ipswich, MA). The primers used were as follows:

Y118A*CLPP* fwd: 5' gagagcaacaagaagcccatccacatggccatcaacagccctggtggtgtggtgacc 3'

Y118A*CLPP* rev: 5'ggtcaccacaccaccagggctgttgatggccatgtggatgggcttcttgttgctctc 3'

D190A*CLPP* fwd: 5'ggccaagccacagccattgccatccagg 3'

D190A*CLPP* rev: 5' cctggatggcaatggctgtggcttggcc 3'

For *in vitro* experiments, mutant genes without mitochondrial targeting sequence (MTS) were fused in frame with N-terminal His6-SUMO-2 tags in pETSUMO2 expression vectors. For experiments involving mammalian cells lines, full length mutant genes

(with MTS) were cloned into an expression vector with a C-terminal VA-tag (StrepIII-His6-TEV-TEV-3xFLAG). All mutations were confirmed by sequencing.

Immunoblot Analysis

Cells were lysed at a density of 1 x 10^6 /50 μL (for AML cells) or 1 x 10^6 /100 μL (for HCT116 cells) in protein lysis buffer (0.25 M Tris-HCl, 2% sodium dodecylsulfate, 4% β-mercaptoethanol, 10% glycerol, 0.02% bromophenol blue). Protein lysates for Oxphos cocktail antibodies were incubated for 30 min at room temperature, otherwise, at 95°C for 5 min for denaturing (antibodies used are listed below). Immunoblot analysis was performed as reported previously (Ishizawa et al., 2016). Briefly, an equal amount of protein lysate was loaded onto a 10-12% SDS-PAGE gel (Bio-Rad), and quantitated using the Odyssey imaging system (LI-COR Biotechnology, Lincoln, NE). Antibodies used: total OXPHOS rodent WB antibody cocktail, anti-SDHA, anti-SDHB, anti-NDUFA12, anti-ClpP, anti-ATF4, anti-eIF2α, anti-phospho-eIF2a (S51) , anti-ClpP, anti-CQCRC2, anti-CS, anti-NDUFB8, anti-β-actin, and anti-GAPDH.

Proximity-Dependent Biotin Labeling (BioID)

Wild-type and Y118A mutant *CLPP* sequences were PCR amplified and fused in-frame with a mutant *E. coli* biotin conjugating enzyme, BirA R118G (or BirA*), in a pcDNA5 FRT/TO plasmid under a CMV promoter positively regulated by tetracycline. For each construct, in-frame fusion was confirmed by Sanger Sequencing. The plasmids were then transfected into T-REx 293 cells using PolyJet (3ul) (SignaGen, Rockville, MD). Stable cells expressing the tetracycline-regulated, BirA*-tagged WT or constitutively active mutant ClpP proteins were selected using hygromycin B (200 μg/mL). Cell pools expressing the BirA* epitope tag alone, or BirA* fused to the unrelated mitochondrial enzyme ornithine transcarbamoylase (OTC) were used as negative controls.

At approximately 60% confluence, cells were treated with 1 μg/ml tetracycline and 50 μM biotin in addition to 0.6μM ONC201 or vehicle control for 48h. Cells were scraped in their media, pooled and washed twice in 25 ml cold PBS, pelleted by centrifugation at 1000 × *g* for 5 min at 4°C, and lysed in ice-cold modified RIPA buffer for 1. Pure cell lysates were then incubated with RIPA-equilibrated streptavidin-sepharose beads (GE Healthcare, Little Chalfont, UK) in an end-over-end rotator for 2 hr at 4°C. Beads were washed seven times with 1 mL of 50 mM ammonium bicarbonate (pH 8.0) and the biotinylated proteins were digested with trypsin. Two separate biological replicates (starting from the cloning phase) were generated for WT ClpP (treated and untreated) and each mutant. Samples containing the peptide fragments were analyzed by mass spectrometry.

Mass Spectrometry Analysis

High performance liquid chromatography was conducted using a 2-cm pre-column (Acclaim PepMap™ 100; 75 μm ID; 3 μm, 100 Å C18; ThermoFisher Scientific, Waltham, MA) and a 50-cm analytical column (Acclaim® PepMap RSLC, 75 μm ID; 2 μm, 100 Å C18; ThermoFisher Scientific, Waltham, MA), applying a 120-min reversed-phase gradient (225nl/min, 5-40% CH_3CN in 0.1% HCOOH) on an EASY-nLC1000 pump (ThermoFisher Scientific, Waltham, MA) in-line with a Q-Exactive HF mass spectrometer (ThermoFisher Scientific, Waltham, MA). A parent ion MS scan was performed at a resolution of 60,000 (FWHM at 200 *m/z*), followed by up to 20 MS/MS scans (15,000 FWHM resolution, minimum ion count of 1000 for activation) of the most intense MS scan ions using higher energy collision induced dissociation (HCD) fragmentation.

Dynamic exclusion was activated such that MS/MS of the same *m/z* (within a range of 10 ppm; exclusion list size = 500) detected twice within 5 sec was excluded from analysis for 15 sec. For protein identification, Thermo .RAW files were converted to the .mzML format using Proteowizard(Kessner et al., 2008), then searched using X!Tandem(Craig and Beavis, 2004) and Comet(Eng et al., 2013) against the Human RefSeq Version 45 database (containing 36113 entries). Search parameters specified a parent ion mass tolerance of 10 ppm, and an MS/MS fragment ion tolerance of 0.4 Da, with up to 2 missed cleavages allowed for trypsin. Variable modifications of +16@M and W, +32@M and W, +42@N-terminus, and +1@N and Q were allowed. Proteins identified with an iProphet cut-off of 0.9 (corresponding to $\leq$ 1% FDR) and at least two unique peptides were analyzed with SAINT Express v.3.6. Control runs (18 runs from cells expressing the FlagBirA* epitope tag only) were collapsed to the two highest spectral counts for each prey, and high confidence interactors were defined as those with BFDR $\leq$ 0.01.

Network Analysis

ClpP interaction data were imported into Cytoscape 3.6.0, and proteins grouped according to previously reported physical interaction and functional data.

Lentiviral Infection and ClpP Over-expression

A lentiviral WT or D190A mutant ClpP-over-expressing vector was generated by amplifying the cDNA by using primers *CLPP* cDNA fwd and *CLPP* cDNA rev (listed below) from Z138 cells and inserting it by InFusion cloning (TaKaRa Bio USA, Mountain View, CA) between the EcoR1 and BamH1 sites of pCDH-EF1a-MCS-BGH-PGK-GFP-T2A-Puro (Systems Biosciences, Palo Alto, CA) by using primers InFusion *CLPP* fwd and InFusion *CLPP* rev. We then derived *CLPP* D190A from the wild type vector using paired primers (*CLPP* mut D190A fwd and *CLPP* mut D190A rev) with a QuikChange II site directed mutagenesis kit (Agilent Technologies, Santa Clara, CA). We followed the manufacturer's method except that used Stbl3 cells (ThermoFisher, Waltham, MA) in lieu of XL10-Gold. We identified the correct clones by Sanger sequence analysis. The sequences of all primers used to construct plasmids are listed in the Key Resources Table.

A tetracycline-inducible system based on two lentiviral vectors was developed as we previously described (Frolova et al., 2012). The first lentiviral vector (pCD510-rtTA) was generated by excising the reverse tetracycline-controlled transactivator (rtTA) coding sequence from pSLIK-Venus-TmiR-Luc (ATCC ID: MBA-239) with BamHI and BstBI and cloning the resulting fragment into NotI and BstBI restriction sites of pCD510-B1 (SystemBio). Thus, pCD510-rtTA expresses rtTA under the CMV promoter and Puromycin selection marker under a second promoter EF-1. To generate the second vector (pCD550A1-TRE), we replaced the original EF1 promoter by an inducible promoter composed of six tetracycline responsive elements (TRE) followed by the minimal CMV promoter. cDNA sequence of WT or Y118A mutant *CLPP* was inserted under the control of a tetracycline inducible promoter (TRE) followed by the minimal CMV promoter and CopGFP, as selection marker, under the control of the EF-1 promoter. For lentiviral infections, HEK293T cells (ATCC, Manassas, VA) were co-transfected with pMD2.G and psPAX2 (kind gifts of Didier Trono, plasmids 12259 and 12260, respectively, Addgene Inc., Cambridge, MA) along with the lentiviral vectors using JetPrime transfection reagent (VWR, Radnor, PA) according to the manufacturer's protocol. The transfection medium was replaced after 6 h with fresh DMEM medium with 10% FBS and 24 h later the viral supernatants were collected and concentrated by using Centricon Plus-70 filter units (Sigma-Aldrich). OCI-AML3, Z138 and HCT116 cells were infected overnight with viral supernatants supplemented with 8 μg/ml of Polybrene (Sigma-Aldrich). Seventy-two h after infection stably transduced cells were selected by FACS resulting in a homogeneous population of GFP-labeled cells.

Measurement of Oxygen Consumption Rate

Oxygen consumption was measured using a Seahorse XF96 analyzer (Seahorse Bioscience, North Billerica, MA). Cells were treated with increasing concentrations of ONC201 or vehicle control (DMSO) in their growth medium for 72 hr at 37°C, resuspended in XF Assay medium supplemented with 2.0 g/l glucose and 100 mM pyruvate, and seeded at 1 x 10^5 cells/well in XF96 plates. Cells were then equilibrated to the un-buffered medium for 60 min at 37°C in a CO_2-free incubator and transferred to the XF96 analyzer. To measure the spare reserve capacity of mitochondrial respiratory chains, cells were treated with 2 μM oligomycin and 0.25 μM carbonyl cyanide *p*-trifluoromethoxyphenylhydrazone (FCCP) in succession.

Respiratory Chain Complexes Activity

Enzymatic activities of respiratory chain complexes were measured as previously described (Sriskanthadevan et al., 2015). NADH-dependent activity of complex I was determined using Complex I Enzyme Activity Microplate Assay Kit in whole cell lysates following oxidation of NADH to NAD^+ and simultaneous reduction of the provided dye. Complex II (succinate dehydrogenase) activity was measured in 2 μg isolated mitochondria in 20 mM sodium succinate-supplemented 100 mM HEPES, pH 7.4 containing 1 mg/mL bovine serum albumin, 20 μM rotenone, and 2mM KCN by monitoring malonate-sensitive reduction of 170 μM 2,6-dichloroindophenol when coupled to complex II-catalyzed reduction of 50 μM decylubiquinone (Skrtic et al., 2011). Complex IV activity was measured by KCN-sensitive oxidation of 2 mg/mL ferrocytochrome *c* in 3 μg isolated mitochondria treated with 1 mg/mL dodecyl-D-maltoside in 25 mM Tris buffer, pH 7.0 supplemented with 125 mM KCl. Ferrocytochrome *c* was obtained by reduction of 40 mg/mL ferricytochrome *c* with 0.5 M L-ascorbic acid (Skrtic et al., 2011).

Mitochondrial ROS Measurement

To measure reactive oxygen species level in mitochondrial, cells were treated with ONC201 (0-2.5 μM) for 72 hr at 37°C, stained with MitoSox (Molecular Probes/Life Technologies, Eugene, OR), and incubated in the dark for 30 min at 37°C and 5% CO2 in humidified atmosphere. Cells were then centrifuged to remove the dye and resuspended in binding buffer containing annexin V-FITC (BioVision, Milpitas, CA). Following this step, annexin V negative cells were identified and analyzed by flow cytometry in a Canto II 96 well cytometer (Fortessa system, Becton Dickinson, San Jose, CA). Positive control samples were treated with 50 μM antimycin A (Sigma-Aldrich) at 37°C 5 h before staining with MitoSox.

QUANTIFICATION AND STATISTICAL ANALYSIS

Statistical analyses were performed using the two-tailed Student's *t* test, One-way ANOVA or Mann-Whitney test by the Prism (version 7.0; GraphPad Software) statistical software programs. The Kaplan-Meier method was used to generate survival curves, and log-rank test was used for comparison of the two groups. A p value < 0.05 was considered statistically significant.

DATA AND SOFTWARE AVAILABILITY

All raw mass spectrometry files have been deposited at the MassIVE archive (massive.ucsd.edu), accession ID# MSV000082381.

The structure of the human mitochondrial ClpP in complex with ONC201 was deposited into the RCSB - Protein Data Bank (PDB) under the accession number 6DL7.

All RNA-seq raw data have been deposited at the Sequence Read Archive (SRA), accession ID# SUB4176298.

Cancer Cell, Volume *35*

Supplemental Information

Mitochondrial ClpP-Mediated Proteolysis Induces Selective Cancer Cell Lethality

Jo Ishizawa, Sarah F. Zarabi, R. Eric Davis, Ondrej Halgas, Takenobu Nii, Yulia Jitkova, Ran Zhao, Jonathan St-Germain, Lauren E. Heese, Grace Egan, Vivian R. Ruvolo, Samir H. Barghout, Yuki Nishida, Rose Hurren, Wencai Ma, Marcela Gronda, Todd Link, Keith Wong, Mark Mabanglo, Kensuke Kojima, Gautam Borthakur, Neil MacLean, Man Chun John Ma, Andrew B. Leber, Mark D. Minden, Walid Houry, Hagop Kantarjian, Martin Stogniew, Brian Raught, Emil F. Pai, Aaron D. Schimmer, and Michael Andreeff

A

S. Aureus ClpP: Q I D D N V A N S I V S Q L L F L Q A Q D S E K D I Y L - - Y (63) I N S P G G S V T A G

Human ClpP: P I D D S V A S L V I A Q L L F L Q S E S N K K P I H M E T Y (118) I N S P G G V V T A G

B

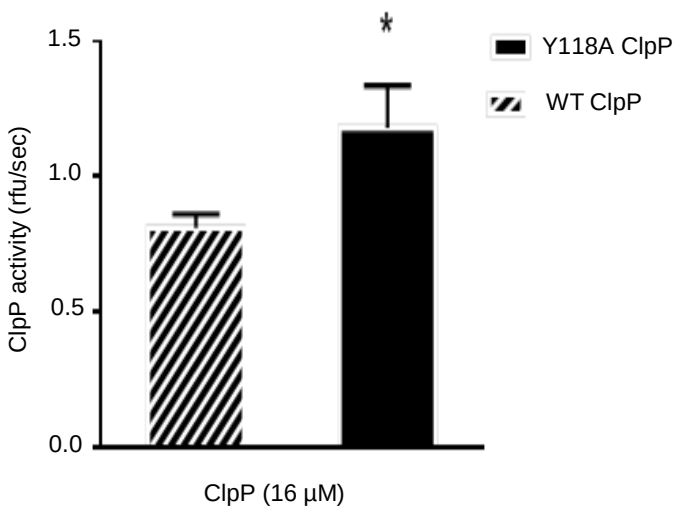

Figure S1. Related to Figure 1. An activating mutation Y118A in ClpP activates recombinant WT ClpP in vitro.

(A) Sequence alignment of S. aureus and human ClpP.

(B) FITC-casein degradation rates of WT ClpP and Y118A ClpP mutants. The results are expressed as the mean of triplicate samples ± SD (error bars). *$p < 0.05$.

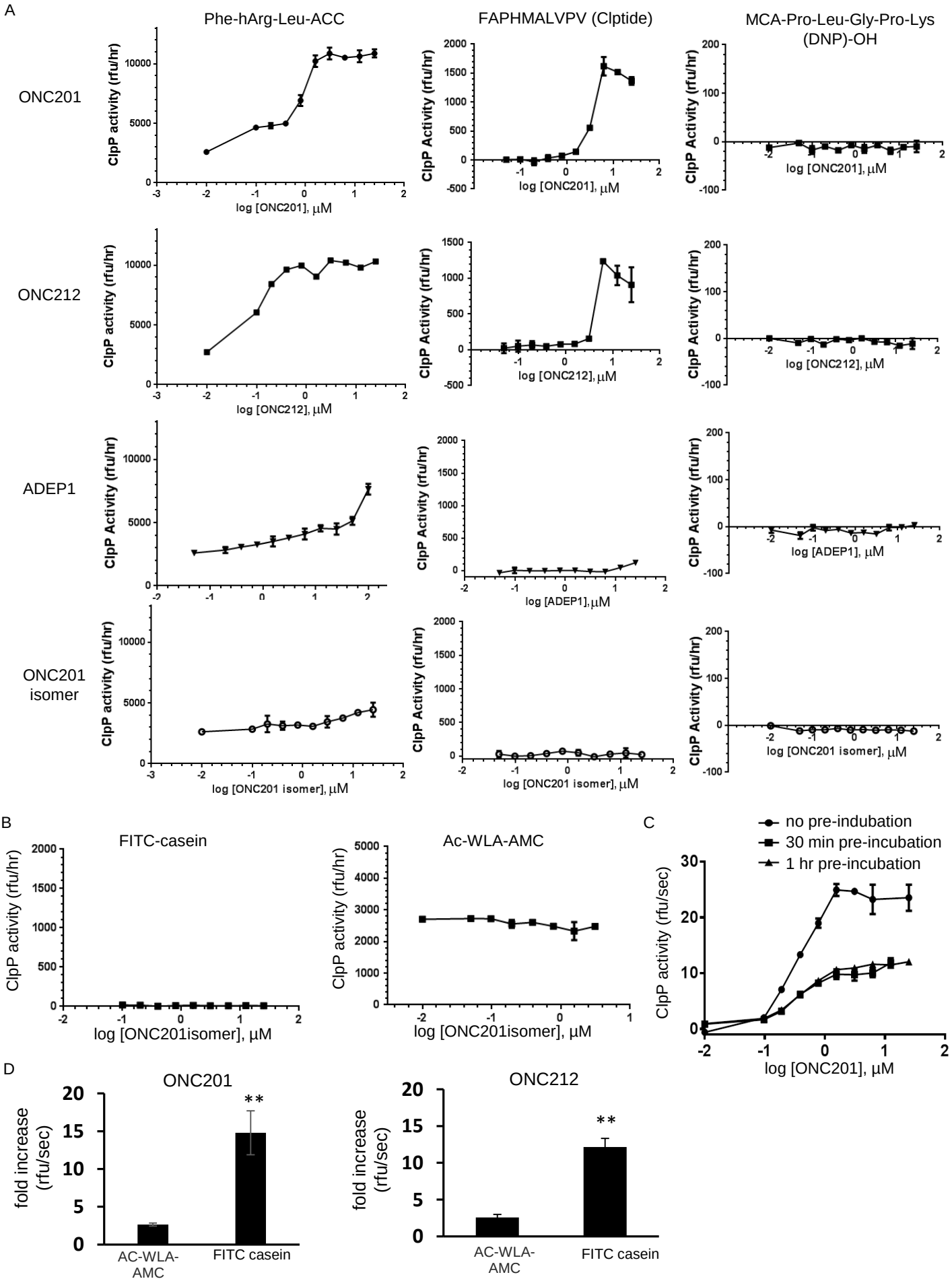
A
Phe-hArg-Leu-ACC
FAPHMALVPV (Clptide)
MCA-Pro-Leu-Gly-Pro-Lys (DNP)-OH
ONC201
ONC212
ADEP1
ONC201 isomer
ClpP activity (rfu/hr)
ClpP Activity (rfu/hr)
log [ONC201], μM
log [ONC212], μM
log [ADEP1], μM
log [ONC201 isomer], μM
B
FITC-casein
Ac-WLA-AMC
ClpP activity (rfu/hr)
log [ONC201isomer], μM
C
no pre-indubation
30 min pre-incubation
1 hr pre-incubation
ClpP activity (rfu/sec)
log [ONC201], μM
D
ONC201
ONC212
fold increase (rfu/sec)
**
AC-WLA-AMC
FITC casein

Figure S2. Related to Figure 2. Imipridones activate recombinant WT ClpP in vitro.

(A) Effects of ONC201, ONC212, ADEP1 and ONC201 inactive isomer on degradation of fluorogenic substrates (Phe-hArg-Leu-ACC, Clptide, and MCA-Pro-Leu-Gly-Pro-Lys (DNP)-OH) by WT ClpP. The results are expressed as the mean of triplicate samples ± SD (error bars).

(B) Effects of ONC201 inactive isomer on degradation of FITC-casein (left) and Ac-WLA-AMC (right) by recombinant WT ClpP. The results are expressed as the mean of triplicate samples ± SD (error bars).

(C) Effect of pre-incubation of WT ClpP with ONC201 (0-60 min) on degradation rate of FITC-casein. The results are expressed as the mean of triplicate samples ± SD (error bars).

(D) Effects of ONC201 and ONC212 on degradation of fluorogenic substrates (AC-WLA-AMC and FITC-casein) by WT ClpP. The results are expressed as the mean of triplicate samples ± SD (error bars). **$p < 0.01$.

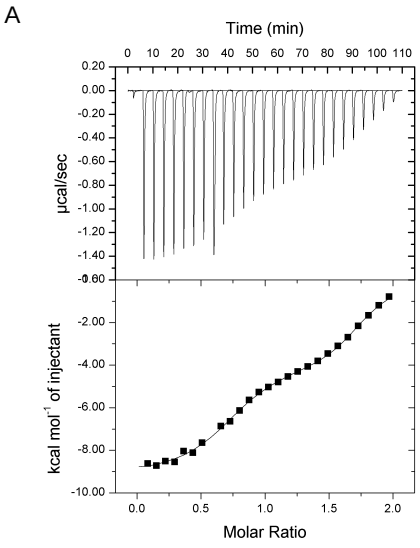
A
Time (min)
µcal/sec
kcal mol⁻¹ of injectant
Molar Ratio

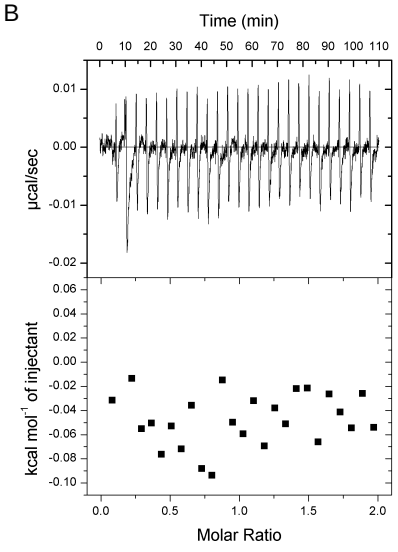
B
Time (min)
µcal/sec
kcal mol⁻¹ of injectant
Molar Ratio

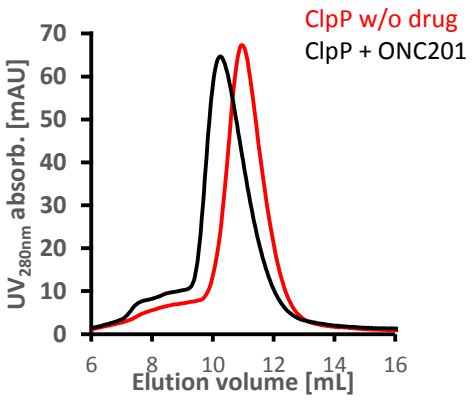
C
ClpP w/o drug
ClpP + ONC201
UV280nm absorb. [mAU]
Elution volume [mL]

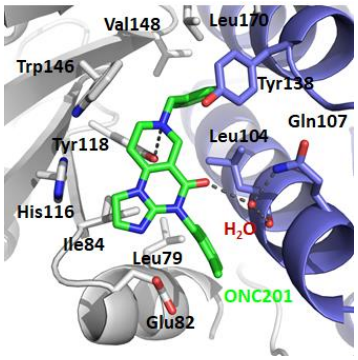
D
Val148
Leu170
Trp146
Tyr138
Gln107
Tyr118
Leu104
His116
H2O
Ile84
Leu79
ONC201
Glu82

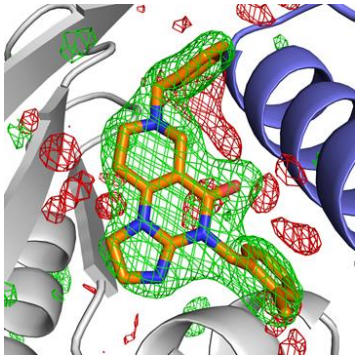
E

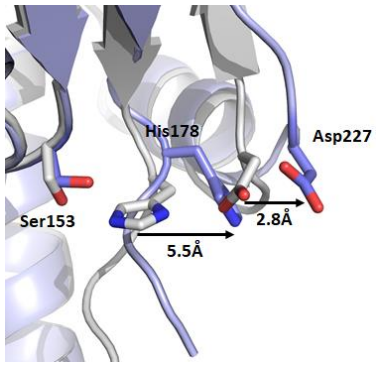
F
His178
Asp227
Ser153
2.8Å
5.5Å

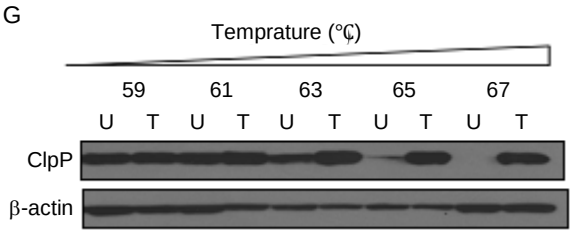
G
Temprature (℃)
59
61
63
65
67
U T U T U T U T U T
ClpP
β-actin

Figure S3. Related to Figure 3. The imipridones bind and activate ClpP, resulting in anti-tumor effects.

(A) Binding of ClpP to ONC201 measured by isothermal calorimetry. 500 μM WT ClpP titrated into 50 μM ONC201.

(B) Control – buffer titrated into 50 μM ONC201.

(C) Gel filtration of ClpP run alone (red) and with equimolar ONC201 (black).

(D) ONC201 in the hydrophobic pocket between two subunits (gray and blue, hydrogen bonds are indicated by dashed lines; a water molecule mediating hydrogen bonding is indicated by a red sphere).

(E) ONC201 and the positive mFo-DFc difference density (green). Map calculated by omitting ONC201 molecules from the structure and contoured at 3σ (ClpP chain A – gray, chain G – violet; negative difference density in red).

(F) Catalytic triad rearrangement upon ONC201 binding to ClpP – both His178 and Asp227 move away from Ser153 (apo – grey; ONC201-bound – violet).

(G) Effect of treatment with 10 uM ONC201 on thermal stability of endogenous ClpP in OCI-AML2 cells tested by CETSA. U: untreated control; T: treated with 10 uM ONC201. Intact cells were treated with ONC201 for 30 min and heated (59-67˚C) for 3min prior to collection of cell lysates for immunoblotting.

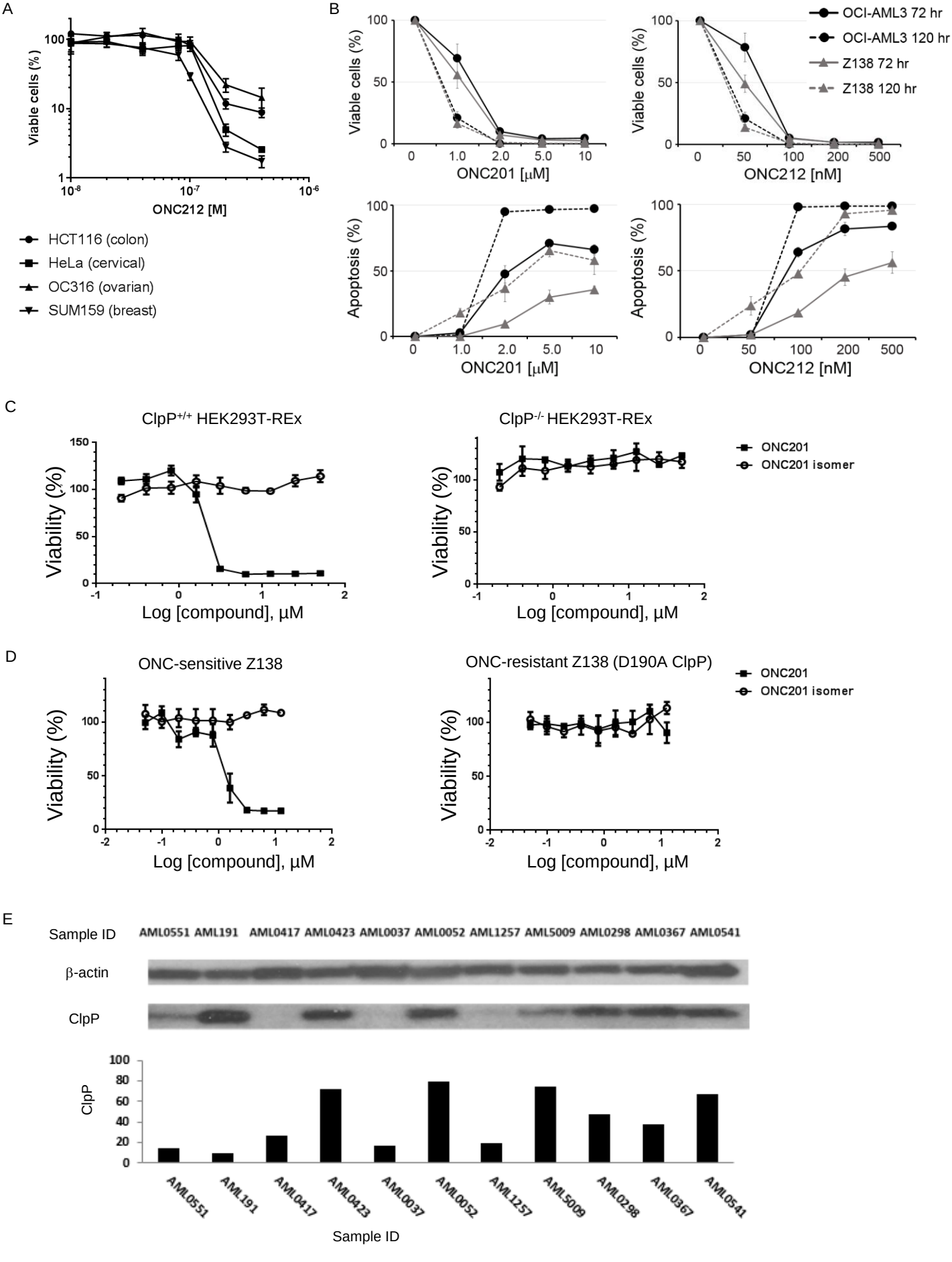
A
Viable cells (%)
ONC212 [M]
HCT116 (colon)
HeLa (cervical)
OC316 (ovarian)
SUM159 (breast)
B
Viable cells (%)
ONC201 [μM]
ONC212 [nM]
OCI-AML3 72 hr
OCI-AML3 120 hr
Z138 72 hr
Z138 120 hr
Apoptosis (%)
C
ClpP+/+ HEK293T-REx
ClpP-/- HEK293T-REx
Viability (%)
Log [compound], μM
ONC201
ONC201 isomer
D
ONC-sensitive Z138
ONC-resistant Z138 (D190A ClpP)
E
Sample ID
AML0551 AML191 AML0417 AML0423 AML0037 AML0052 AML1257 AML5009 AML0298 AML0367 AML0541
β-actin
ClpP

Figure S4. Related to Figure 4. Cytotoxicity of imipridones is ClpP-dependent.

(A) Effects of ONC212 on viability of HCT-116, HeLa, OC316 and SUM159 cells. Data represent percent viable cells measured by annexin V assay after a 72-hr period of exposure to ONC212. The results are expressed as the mean of triplicate samples ± SD (error bars).

(B) Apoptosis in Z138 and OCI-AML3 cells treated with ONC201 and ONC212. Cells were treated with ONC201 or ONC212 at indicated concentrations for 72 or 120 hours. Annexin V- and PI-negative cells were counted as live cells (upper panels), and Annexin V+ cells were counted as apoptotic cells (lower panels), normalized to untreated samples. The results are expressed as the mean of triplicate samples ± SD (error bars).

(C-D) Effects of ONC201 & its inactive isomer on viability in $ClpP^{+/+}$ or $ClpP^{-/-}$ T-REx HEK293 (C) and ONC201-sensitive or ONC201-resistant Z138 (D) cells. Data represent percent mean ± SD (error bars) for viable cells measured by alamar blue assay after a 72-hour period of exposure to the compounds.

(E) Effect of ONC201 on viability of primary AML samples measured by annexin V assay after a 72 hour period of exposure. ClpP expression level in each sample was measured by immunoblot analysis of untreated samples. The bar graph shows the relative expression level of ClpP.

Table S1. Clinical information of samples used for Figure 4.

Sample No.	Gender	Age	Organ	WBC (10^3/mm^3)	Blast (%)	Gene mutations	Cytogenetics	Disease Status
1	M	68	PB	98.7	91	*FLT3-ITD, CEBPA, WT1*	intermediate	Refractory
2 (#)	M	74	PB	8.9	66	*ASXL1, DNMT3A, IDH2, SRSF2, TP53*	High risk (complex)	Refractory
3 (##)	F	36	PB	46.5	90	*DNMT3A, FLT3-ITD, NPM1, IDH2*	High risk (complex)	Relapsed/Refractory
4	F	41	BM	-	77	*PHF6*	High risk (complex)	Relapsed/Refractory
5	F	51	PB	49.9	49	*NRAS, TET*	Intermediate	Relapsed/Refractory
6	M	72	PB	63.1	98	*FLT3, IDH1, NPM1, PRPF40B, SRSF2*	Intermediate (diploid)	Newly Diagnosed
7	F	62	BM	-	87	*KRAS, NRAS*	Intermediate	Newly Diagnosed
8	M	63	BM	-	77	*ASXL1, CSF3R, NF1*	High risk (monosomy 7)	Refractory
9	M	72	BM	-	90	*IDH2, NPM1, SRSF2*	intermediate (diploid)	Newly Diagnosed

#, ##: Samples which were relatively resistant to ONC201 in Figure 4B.

Table S2. Clinical information of samples used for Figure 4.

ID	Age	Gender	Source	Disease Status	WBC (x10e9/L)	PB Blasts (x10e9/L)	BM Blasts (%)	NPM1
AML0367	42	M	PB	Diagnosis	313	291.09	90	-
AML0551	32	M	PB	Diagnosis	145	101.5	85	not done
AML1257	58	M	PB	Diagnosis	189	111	70	Positive
AML0052	73	F	PB	Diagnosis/ Secondary to CMML	60.7	0	20	not done
AML0298	54	M	PB	Diagnosis	97.7	89.88	97	Positive
AML5009	73	F	PB	Diagnosis/ Secondary to MPN	31.3	15.96	48	Negative
AML0541	51	F	PB	Diagnosis	166	151.3	86	Positive
AML0037	24	F	PB	Diagnosis	43.3	12.99	not done	not done
AML191	39	M	BM	Diagnosis	168	159.6	90	not done

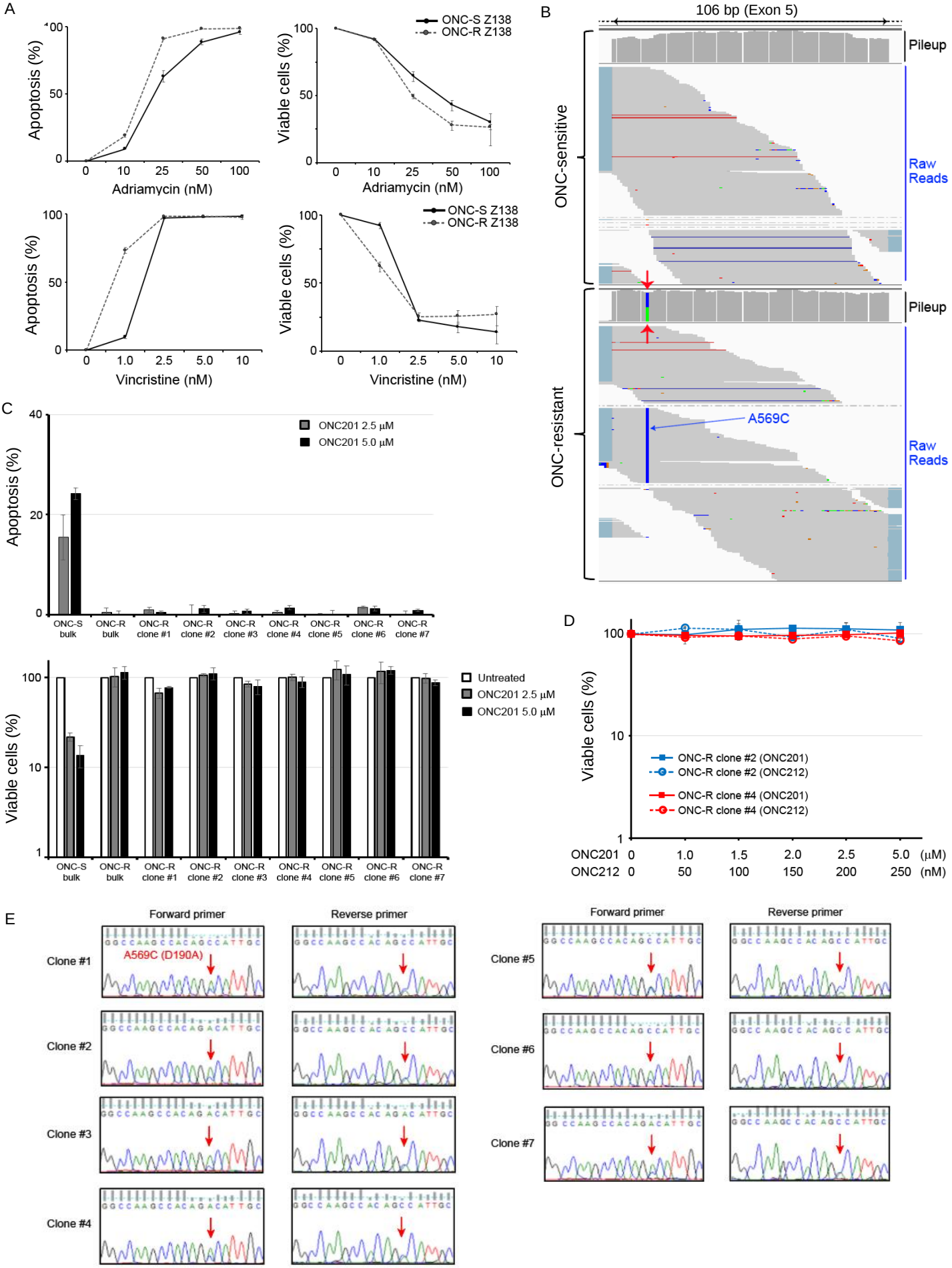
A
Apoptosis (%)
Adriamycin (nM)
Viable cells (%)
ONC-S Z138
ONC-R Z138
Vincristine (nM)
B
106 bp (Exon 5)
Pileup
Raw Reads
ONC-sensitive
ONC-resistant
A569C
C
ONC201 2.5 μM
ONC201 5.0 μM
ONC-S bulk
ONC-R bulk
ONC-R clone #1
ONC-R clone #2
ONC-R clone #3
ONC-R clone #4
ONC-R clone #5
ONC-R clone #6
ONC-R clone #7
Untreated
D
ONC-R clone #2 (ONC201)
ONC-R clone #2 (ONC212)
ONC-R clone #4 (ONC201)
ONC-R clone #4 (ONC212)
ONC201 0 1.0 1.5 2.0 2.5 5.0 (μM)
ONC212 0 50 100 150 200 250 (nM)
E
Forward primer
Reverse primer
Clone #1
A569C (D190A)
Clone #2
Clone #3
Clone #4
Clone #5
Clone #6
Clone #7

Figure S5. Related to Figure 5. ONC201-resistant single-cell clones were resistant to ONC201 and ONC212 and harbored a heterozygous D190A mutation.

(A) Sensitivity of ONC201-resistant cells to standard chemo-agents. ONC201-resistant Z138 cells (clone #2) were treated with Adriamycin (upper panels) and Vincristine (lower panels) at indicated concentrations for 72 hours. Annexin V-positive cells (left) and Annexin V/PI double negative cells (right) were measured by flow cytometry. The results are expressed as the mean of triplicate samples ± SD (error bars).

(B) Result of RNA sequencing of parental (ONC-sensitive) and ONC-resistant Z138 cells. Individual reads are visualized below for each cell line, and above bar graphs indicate the number of reads ("pileup") at each nucleotide of the genomic exon sequence. Red arrows indicate the position of wild-type A569 (green) and A569C mutation (blue).

(C) Sensitivity of single cell clones of ONC201-resistant Z138 cells to ONC201. Single cell clones derived from ONC201-resistant Z138 cells were treated with ONC201 at indicated concentrations for 72 hours. Apoptotic cells (annexin V-positive) cells (upper) and live (Annexin V- and PI-double negative) cells (lower) were measured by flow cytometry. The results are expressed as the mean of triplicate samples ± SD (error bars).

(D) Sensitivity of single-cell clones #2 and #4 derived from ONC201-resistant Z138 cells to ONC201 and ONC212 was assessed by Annexin V assays. Data represent percent viable (annexin V and PI double negative) cells. The results are expressed as the mean of triplicate samples ± SD (error bars).

(E) Sanger sequence of genomic DNA, related to Figure 4B. A D190A heterozygous mutation was detected in all the tested 7 single- cell clones.

A

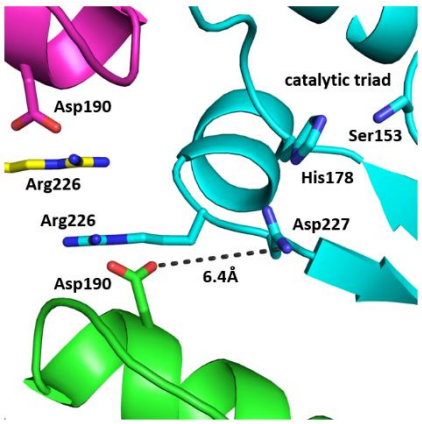
catalytic triad
Asp190
Ser153
Arg226
His178
Arg226
Asp227
6.4Å
Asp190

B

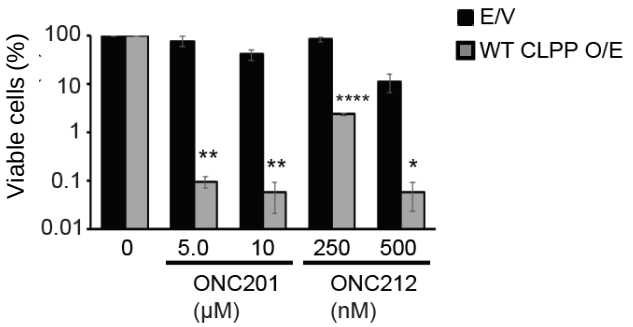
E/V
WT CLPP O/E
Viable cells (%)
100
10
1
0.1
0.01
**
**
****
*
0
5.0
10
250
500
ONC201
(μM)
ONC212
(nM)

C

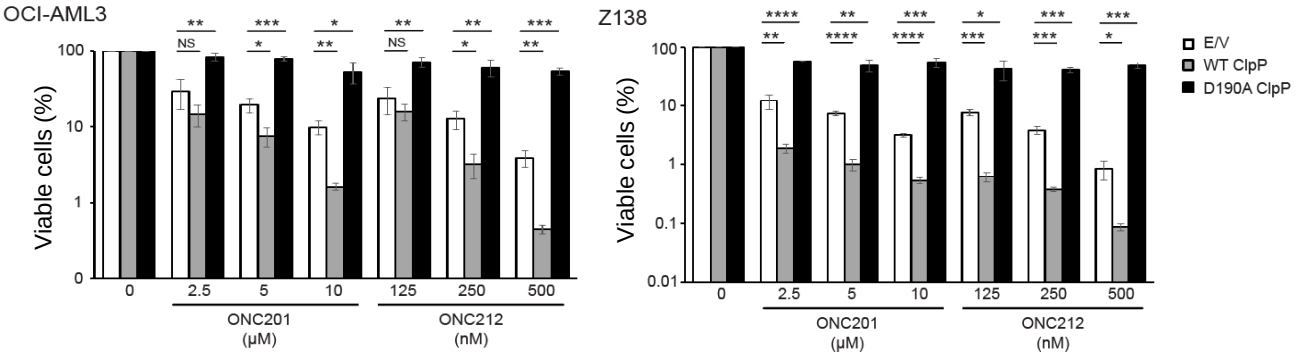
OCI-AML3
Z138
E/V
WT ClpP
D190A ClpP
Viable cells (%)
100
10
1
0.1
0.01
0
0
2.5
5
10
125
250
500
ONC201
(μM)
ONC212
(nM)
NS

D

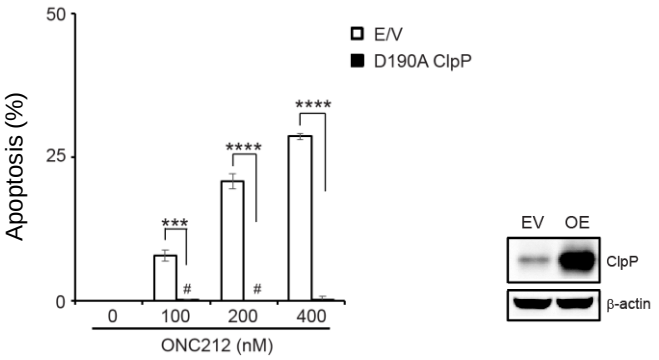
E/V
D190A ClpP
Apoptosis (%)
50
25
0
***
****
****
#
#
0
100
200
400
ONC212 (nM)
EV
OE
ClpP
β-actin

Figure S6. Related to Figure 5. D190A mutation in ClpP renders tumor cells resistant to imipridones.

(A) The location of D190 and Asp227 in the 3-D structure of an apparently closed conformation of human mitochondrial ClpP. D227 (Asp227) is 6.4 angstroms away from D190 and part of the catalytic triad of ClpP.

(B-C) Changes in live cell number by ONC201 and ONC212 on ClpP-overexpressed Z138 and OCI-AML3 cells. Viable cells were measured by flow cytometry. (C) WT ClpP over-expressing ONC201-resistant Z138 cells. Data represent percent viable (annexin V and PI double negative) cells. (D) WT or D190A ClpP over-expressing OCI-AML3 and Z138 cells. The results are expressed as the mean of triplicate samples ± SD (error bars). *P < 0.05, **P < 0.01, ***P < 0.001, ****P < 0.0001.

(D) Overexpression of D190A-ClpP in HCT116 cells. Cells were treated with ONC201 and ONC212 at indicated concentrations for 72 hours. Data represent percent apoptotic (annexin V-positive) cells. The results are expressed as the mean of triplicate samples ± SD (error bars). ***P < 0.001, ****P < 0.0001. Protein expression levels of ClpP were assessed by immunoblotting. EV; empty vector, OE; overexpression. #; invisible bars because of low numerical values.

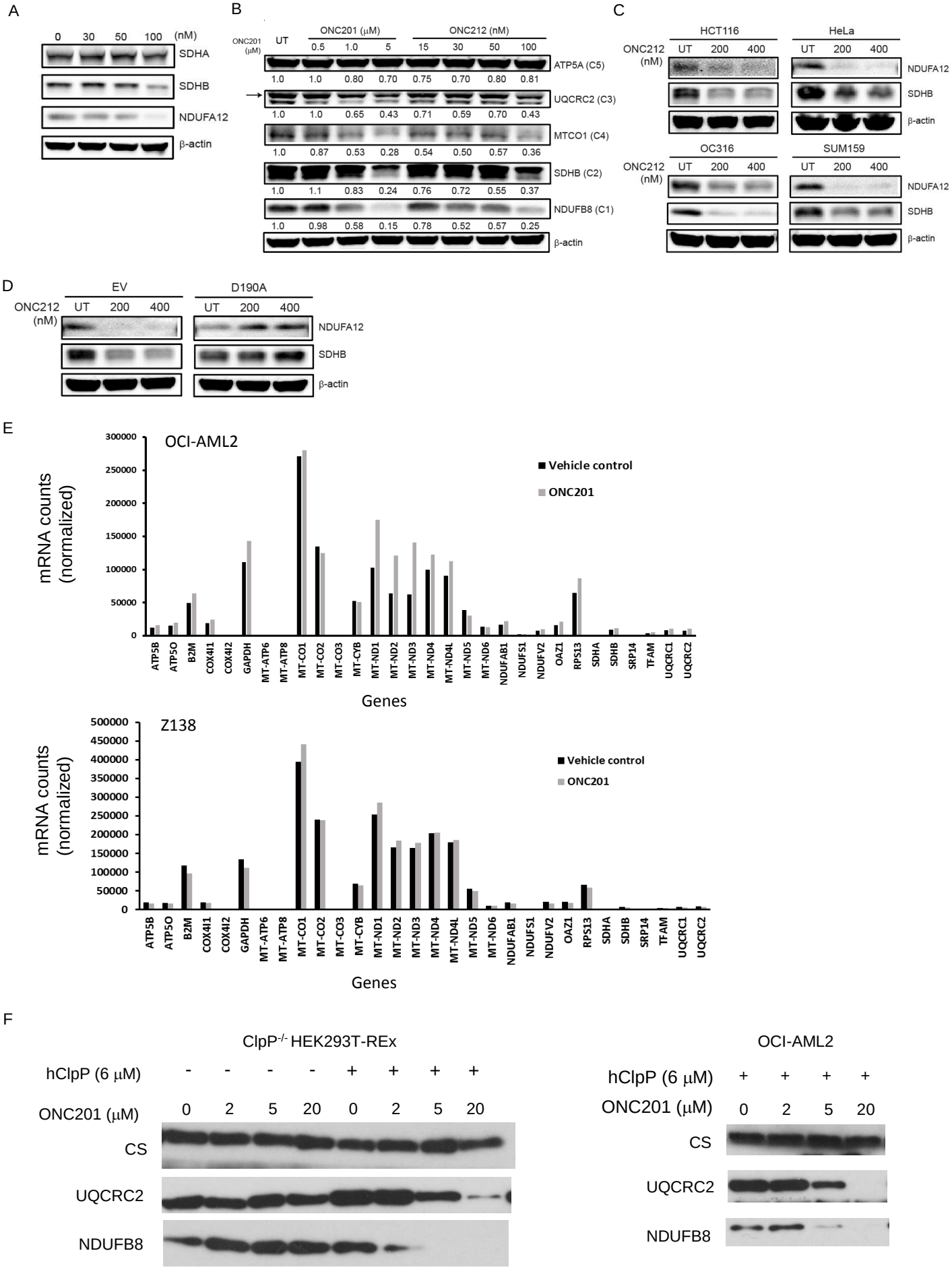
A
0 30 50 100 (nM)
SDHA
SDHB
NDUFA12
β-actin
B
ONC201 (μM)
UT
ONC201 (μM)
0.5 1.0 5
ONC212 (nM)
15 30 50 100
ATP5A (C5)
1.0 1.0 0.80 0.70 0.75 0.70 0.80 0.81
UQCRC2 (C3)
1.0 1.0 0.65 0.43 0.71 0.59 0.70 0.43
MTCO1 (C4)
1.0 0.87 0.53 0.28 0.54 0.50 0.57 0.36
SDHB (C2)
1.0 1.1 0.83 0.24 0.76 0.72 0.55 0.37
NDUFB8 (C1)
1.0 0.98 0.58 0.15 0.78 0.52 0.57 0.25
β-actin
C
HCT116
HeLa
ONC212 (nM)
UT 200 400
NDUFA12
SDHB
β-actin
OC316
SUM159
D
EV
D190A
ONC212 (nM)
UT 200 400
NDUFA12
SDHB
β-actin
E
OCI-AML2
mRNA counts (normalized)
Vehicle control
ONC201
300000
250000
200000
150000
100000
50000
0
ATP5B ATP5O B2M COX4I1 COX4I2 GAPDH MT-ATP6 MT-ATP8 MT-CO1 MT-CO2 MT-CO3 MT-CYB MT-ND1 MT-ND2 MT-ND3 MT-ND4 MT-ND4L MT-ND5 MT-ND6 NDUFAB1 NDUFS1 NDUFV2 OAZ1 RPS13 SDHA SDHB SRP14 TFAM UQCRC1 UQCRC2
Genes
Z138
mRNA counts (normalized)
Vehicle control
ONC201
500000
450000
400000
350000
300000
250000
200000
150000
100000
50000
0
ATP5B ATP5O B2M COX4I1 COX4I2 GAPDH MT-ATP6 MT-ATP8 MT-CO1 MT-CO2 MT-CO3 MT-CYB MT-ND1 MT-ND2 MT-ND3 MT-ND4 MT-ND4L MT-ND5 MT-ND6 NDUFAB1 NDUFS1 NDUFV2 OAZ1 RPS13 SDHA SDHB SRP14 TFAM UQCRC1 UQCRC2
Genes
F
ClpP-/- HEK293T-REx
hClpP (6 μM) - - - - + + + +
ONC201 (μM) 0 2 5 20 0 2 5 20
CS
UQCRC2
NDUFB8
OCI-AML2
hClpP (6 μM) + + + +
ONC201 (μM) 0 2 5 20
CS
UQCRC2
NDUFB8

Figure S7. Related to Figure 6. ClpP activation induces apoptosis following reduction of respiratory chain complex subunits.

(A) Immunoblot of SDHA, SDHB and NDUFA12 in OCI-AML3 cells treated with ON212 for 24 hours at indicated concentrations.

(B) Immunoblot of respiratory chain complex subunits. OCI-AML3 cells were treated with ONC201 or ONC212 at indicated concentrations for 24 hours.

(C) Immunoblot of SDHB and NDUFA12 in HCT-116, HeLa, OC316 and SUM159 cells treated with ON212 for 24 hours at indicated concentrations.

(D) Immunoblot analysis of respiratory chain complex subunits in HCT116 cells with over-expression of D190A mutant ClpP or an empty vector (EV).

(E) Effect of ONC201 (0.6 μM) on levels of mRNA encoding mitochondrial respiratory chain subunits in OCI-AML2 and Z138 cells.

(F) Immunoblots of citrate synthase (CS), UQCRC2 (complex III), and NDUFB8 (complex I) in mitochondrial lysates isolated from ClpP -/- HEK293T-REx and OCI-AML2 cells treated with increasing concentrations of ONC201 with or without recombinant ClpP (6 μM) after a brief (3-hr) period of incubation.

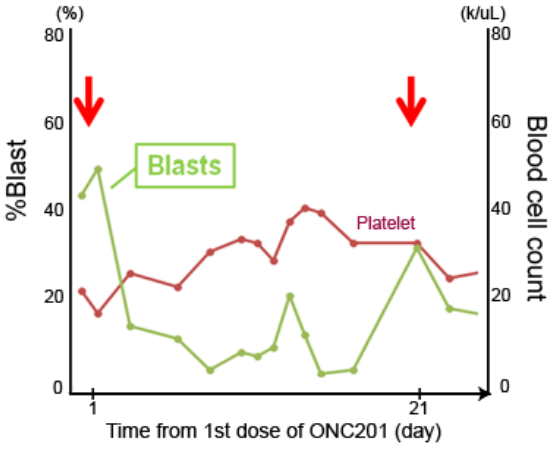
(%)
(k/uL)
80
60
40
20
0
%Blast
Blood cell count
Blasts
Platelet
1
21
Time from 1st dose of ONC201 (day)

Figure S8. Related to Figure 8. ClpP activation exerts anti-tumor effects in vivo.

A patient with AML refractory to decitabine, fludarabine, cyarabine and two investigational IDH2 inhibitors was enrolled in the Phase 1 trial of ONC201. Blasts (50% to 3%) and platelet transfusion requirements were reduced after oral administration of a single dose of ONC201 (250 mg). Arrows indicate ONC201 administration.

Table S4. Related to STAR Methods. Data collection and refinement statistics for ClpP ONC201 complex.

Wavelength	0.97949 Å
Resolution range (Å)	49.4 - 2.0 (2.07 - 2.0)
Space group	C 1 2 1
Unit cell (a, b, c (Å); α, β, γ (°))	142.4 153.4 104.8 90 117.6 90
Total reflections	635237 (63647)
Unique reflections	133979 (13336)
Multiplicity	4.7 (4.8)
Completeness (%)	1.00 (1.00)
Mean I/sigma(I)	5.64 (0.81)
Wilson B-factor	37.1
R-merge	0.149 (1.58)
R-meas	0.168 (1.78)
CC1/2	0.994 (0.504)
CC*	0.998 (0.819)
Reflections used in refinement	133638 (13076)
Reflections used for R-free	6704 (668)
R-work	0.2297 (0.3920)
R-free	0.2622 (0.3902)
CC(work)	0.948 (0.697)
CC(free)	0.933 (0.704)
Number of non-hydrogen atoms	10643
macromolecules	9687
ligands	203
Protein residues	1244
RMS(bonds)	0.01
RMS(angles)	0.57
Ramachandran favored (%)	96
Ramachandran allowed (%)	3.8
Ramachandran outliers (%)	0.25
Rotamer outliers (%)	2.3
Clashscore	1.56
Average B-factor	49.7
macromolecules	49.5
ligands	46.9
solvent	53
Number of TLS groups	1

Statistics for the highest-resolution shell are shown in parentheses. R_{free} is the cross-validation R-factor computed for a test set of reflections not used in the refinement (5 % of total)